HHS Public Access

Author manuscript

Cancer Immunol Res. Author manuscript; available in PMC 2023 October 03.

Published in final edited form as:

Cancer Immunol Res. 2023 April 03; 11(4): 466–485. doi:10.1158/2326-6066.CIR-22-0927.

Combination IFNβ and membrane-stable CD40L maximize tumor dendritic cell activation and lymph node trafficking to elicit systemic T-cell immunity

Hong Zheng[1], **Xiaoqing Yu**[2], **Mohammed L. Ibrahim**[1,7], **Dana Foresman**[1], **Mengyu Xie**[1], **Joseph O. Johnson**[3], **Theresa A. Boyle**[4,5], **Brian Ruffell**[1], **Bradford A. Perez**[6], **Scott J. Antonia**[8], **Neal Ready**[8], **Andreas N. Saltos**[5], **Mark J. Cantwell**[9], **Amer A. Beg**[1,5]

[1]Department of Immunology, Moffitt Cancer Center, Tampa, FL 3362, USA.

[2]Department of Biostatistics and Bioinformatics, Moffitt Cancer Center, Tampa, FL 3362, USA.

[3]Department of Analytical Microscopy, Moffitt Cancer Center, Tampa, FL 3362, USA.

[4]Department of Pathology, Moffitt Cancer Center, Tampa, FL 3362, USA.

[5]Department of Thoracic Oncology, Moffitt Cancer Center, Tampa, FL 3362, USA.

[6]Department of Radiation Oncology, Moffitt Cancer Center, Tampa, FL 3362, USA.

[7]Department of Biochemistry, Faculty of Pharmacy, Cairo University, Cairo, Egypt.

[8]Duke Cancer Institute, Duke University School of Medicine, Durham, NC, North Carolina.

[9]Memgen Inc., 12 Greenway Plaza, Suite 1100, Houston, TX 77046, USA.

Abstract

Oncolytic virus therapies induce direct killing of tumor cells and activation of conventional dendritic cells (cDCs); however, cDC activation has not been optimized with current therapies. We evaluated adenoviral delivery of engineered membrane-stable CD40L (MEM40) and IFNβ to locally activate cDCs in mouse tumor models. Combined tumor MEM40 and IFNβ expression induced the highest cDC activation coupled with increased lymph node migration, increased systemic antitumor $CD8^+$ T-cell responses, and regression of established tumors in a cDC1-dependent manner. MEM40+IFNβ combined with checkpoint inhibitors led to effective control of distant tumors and lung metastases. An oncolytic adenovirus (MEM-288) expressing MEM40+IFNβ in phase 1 clinical testing induced cancer cell loss concomitant with enhanced T-cell infiltration and increased systemic presence of tumor T-cell clonotypes in NSCLC patients.

Correspondence should be addressed to A.A.B at Moffitt Cancer Center, 12902 Magnolia Drive, SRB-2, Tampa Florida 33612. Phone: 813-745-5714. amer.beg@moffitt.org.

Author contributions

Conceptualization was by SJA, MJC, BR, NR, AS and AAB. Methodology was the responsibility of HZ, XY, MLI, MX, CDP and JJ. Writing of the original draft was by HZ, XY, BAP, MJC and AAB. Supervision was performed by NR, AS and AAB. Funding acquisition was by SJA and AAB.

Competing interests

The Moffitt Cancer Center and Memgen have filed patent applications related to this work on which AAB, SJA and MJC are inventors. The patent applications have been licensed to Memgen. AAB and SJA are Memgen Scientific Advisory Board members, MJC is an employee of Memgen. AAB receives grant support from Memgen.

This approach to simultaneously target two major DC-activating pathways has potential to significantly impact the solid tumor immunotherapy landscape.

Keywords

Immunotherapy; T-cell Activation; Dendritic Cells; Oncolytic Virus; Tumor Microenvironment

Introduction

Distinct tumor immune phenotypes vary in their response to currently used immunotherapies (1–4). In general, the “inflamed” tumor phenotype is associated with high T-cell presence in tumors and positive responses to immunotherapies, especially immune checkpoint inhibitors (ICI) (1–4). In contrast, the “immune-desert” or “cold” phenotypes exhibit a virtual absence of T cells in tumor beds, possibly resulting from immune ignorance and/or lack of priming (1–3). Immune desert or immune-excluded phenotypes dominate in many cancer types, resulting in a large unmet need for patients who do not respond well to ICIs. One possible approach to treat these patients is through *in situ* delivered cancer therapies using intralesional/intratumoral (IT) approaches that incorporate stimulators of innate immunity such as STING and TLR agonists, as well as oncolytic viruses (OVs) (5–8). Such *in situ* vaccination approaches provide an opportunity to target conventional dendritic cells (cDCs) in the tumor microenvironment (TME) and trigger activation of a systemic T-cell response (7,9,10).

OVs have been developed for their ability to specifically replicate in cancer cells leading to cell lysis without cytotoxicity in normal cells. The first and currently only FDA approved OV, herpes simplex virus type 1–based talimogene laherparepvec (T-VEC), is currently in use for treatment of melanoma patients through IT administration (7,11–14). Several studies indicate that T-VEC induces an increase in $CD8^+$-T-cell density in non-injected melanoma tumors, consistent with an increase in systemic T-cell immunity (15,16). T-VEC is engineered to express GM-CSF to modulate the activity of myeloid cells, including cDCs, suggesting that in addition to cancer cell lysis to release antigens, modulation of DC activity may also mediate response to T-VEC. However, GM-CSF is not a strong activator of DCs and functions as a general activator of myeloid cells, including those with suppressive functions (17). Hence, optimizing the ability of OVs to activate DCs could improve the therapeutic efficacy of this approach.

Conventional type 1 dendritic cells (cDC1) and conventional type 2 dendritic cells (cDC2) mediate activation of T cells, with cDC1 playing a key role in both $CD8^+$ and $CD4^+$ T-cell activation, whereas cDC2 are more specific for $CD4^+$ T cells in the absence of therapeutic intervention (18–23). cDC1 modulate T-cell activation in both tumor and lymph nodes (18,21,22,24,25), and their presence in tumors correlates with immunotherapy response (26,27). Both cDC1 and cDC2 can differentiate into mature DC with high expression of co-stimulatory molecules, along with expression of T-cell regulatory molecules, and these cells are called mature DCs enriched in immunoregulatory molecules (mregDCs) (28,29).

Finally, the TME can impair DC function suggesting that strategies to activate tumor DCs may be of considerable therapeutic benefit (30,31).

cDC activation is highly regulated by NF-κB and type 1 IFN–induced transcription factors (32,33). CD40 is a cell surface receptor expressed on a variety of antigen-presenting cells (APCs), including cDCs, B cells and macrophages, and is a potent activator of NF-κB (34). Both CD40 and the type 1 IFN pathways have been shown to be crucial for the $CD8^+$ T-cell cross-priming function of cDCs (34–38), and therefore activation of these pathways in the TME could be a promising approach for stimulating antitumor T-cell responses through modulation of cDC function. However, it is not clear which specific aspects of cDC function are regulated by these pathways, whether they have redundant or non-redundant functions in T-cell activation, and how these signals can be safely delivered to the TME without causing systemic toxicity. Herein, we report on the effects of delivering membrane-stable chimeric CD40L (MEM40) (39–41), either alone or in combination with IFNβ, using an adenovirus vector to minimize replication suppression by type 1 IFNs (42). We demonstrate that combined activation of CD40 and type 1 IFN pathways in the TME triggered strong cDC activation and lymph node trafficking, which corresponded to potent induction of systemic $CD8^+$ T-cell immunity and control of both injected and distant tumor growth. These findings demonstrate that the efficacy of OVs can be enhanced by the inclusion of cDC activators. Consistent with these preclinical data, early clinical studies indicate that MEM-288 OV expressing MEM40 + IFNβ transgenes induced tumor cell killing concomitant with a strong increase in T-cell density.

Materials and Methods

Mice and cells

All mice were housed in the animal facility at Moffitt Cancer Center under specific pathogen-free conditions. C57BL/6 and SCID mice were obtained from Charles River (Wilmington, MA), 129S4/SvJaeJ were obtained from Jackson Laboratories (Bar Harbor, ME). $IFNAR1^{-/-}$, $CD40^{-/-}$, $BATF3^{-/-}$ and $CCR7^{-/-}$ mice were obtained from Jackson Laboratories and bred inhouse. All animal experiments were approved by the University of South Florida Institutional Animal Care and Use Committee.

B16-F10 mouse melanoma cell line was from ATCC and was cultured in DMEM (Cat No. 15-017-cv, CORNING) with 10% FBS (Cat No. A52568-01, GIBCO). Zs-Green overexpressing B16-F10 cells were kindly provided by Dr. Max Krummel (University of California, San Francisco). Mouse 344SQ cell line (kindly provided by Dr. J. Kurie, MD Anderson Cancer Center) with KRAS G12D and TP53 mutations (R172H) was maintained in RPMI 1640 (Cat No. 10-040-cv, CORNING) with 10% FBS. Human A549 lung cancer cell line was obtained from the Moffitt Lung Cancer Center of Excellent repository, authenticated by short tandem repeat analysis, and maintained in RPMI 1640 with 10% FBS. For tumor growth studies, cell lines were harvested in logarithmic growth phase after being cultured for less than 2 weeks. Cell lines tested negative for mycoplasma contamination (PlasmoTest, Mycoplasma Detection Kit from InvivoGen, San Diego, CA).

Replication-deficient and oncolytic adenoviruses

Replication-deficient ISF35 adenovirus expressing chimeric membrane-stable CD40L, MEM40, (Ad-MEM40 has been previously described (39–41). Replication-deficient adenoviruses expressing mouse IFNβ (Ad-mIFNβ) human IFNβ (Ad-hIFNβ), mouse GM-CSF (Ad-GMCSF) and control adenovirus Null (Ad-Null) (Supplementary Fig. S1A). were developed with Vector Biolabs (Malvern, PA). The conditionally replicative OV type 5 adenovirus backbone that includes delta-24 (D24) E1, E1b 55kb and E3 viral genome deletions (43,44) was used to generate MEM-288 (Creative Biolabs, Shirley, NY). Briefly, an expression cassette for MEM40 including the cytomegalovirus (CMV) promoter and bovine growth hormone polyadenylation sequences (poly(A)) (45) was inserted upstream of the adenovirus E1 region, and an expression cassette for human IFNβ, including the simian virus 40 (SV40) promoter and poly(A) sequences, was inserted in the E3 region. Ad-GFP was generated with an expression cassette for GFP (including the CMV promoter and poly(A) sequences) inserted upstream of the adenovirus E1 region. All viruses were titered in house using the QuickTiter adenovirus titer immunoassay kit (VPK-109, Cell Biolabs) according to the manufacturer's protocol.

Tumor studies

Cells were harvested in logarithmic growth phase after being cultured for less than 2 weeks, washed once in injection medium (phenol-free DMEM supplemented with 2% FBS), and counted. C57BL/6 mice were inoculated s.c. with 5*e5 B16-F10 cells on the primary site and with 2.5*e5 cells on the contralateral site. The mice were injected with oncolytic or replication-deficient adenoviruses on D12 and 16 into primary tumors or/and with anti-mouse CTLA-4 (Clone UC10-4F10-11, Cat No. BE0032, Bio-X-Cell) and anti-mouse PD-1 (Clone RMP1-14, Cat No. BE0146, Bio-X-Cell) i.p. on D16, D19, D23 and 27 along with matching isotype controls (Cat No. BE0089 and Cat No. BE0091, Bio-X-Cell). Tumors were monitored for growth by measurements 2–3 times per week. The tumor volume was determined as length × width^2/2. Mice were sacrificed when s.c. tumors reached a diameter of 20 mm or when the animals showed signs of morbidity. Similarly, 129S4/SvJaeJ mice were inoculated s.c. with 5*e5 344SQ cells on the flank and injected with oncolytic or replication-deficient adenoviruses on D12 and 16 or/and with anti-PD-1 and CTLA-4 antibodies i.p. on D16, D19, D23 and 27. Mouse lungs were collected and used for H&E and IHC staining. SCID mice were inoculated s.c. with 5*e6 luciferase expressing A549, then injected with 2 doses of oncolytic 10e9 infectious units of Ad-GFP or MEM-288 on D21 and D28 and bioluminescence imaging (BLI) was used to detect tumor growth over 3 weeks.

Flow cytometric analysis

Mice with tumors were cardiac-perfused with PBS containing 10 U/ml heparin to clear peripheral blood, and single cell suspensions were prepared by incubating minced tumor in 1 mg/ml collagenase A (Cat No. 11088793001, Roche) and 50 U/ml DNase I (Cat No. 10104159001, Roche) and with addition of collagenase D (11088882001, Roche) for lymph nodes, at 37°C for 20 mins with agitation, followed by passing through a 70μm cell strainer and lysis of red blood cells (Cat No. BP10-548E, LONZA) for 2 min at room temperature. Immune populations were identified using antibodies described in Supplementary Table S1.

Cells were incubated for 5 mins at room temperature with Fc-block, 30 mins with staining Abs on ice, and DAPI (or L/D near IR fixative viability dye) was added prior to analysis to assess viability. Flow cytometric analysis was performed on BD FACSymphony™ and analyzed using FlowJo software (version 10.7.1, Tree Star). Smaller LNs were pooled and digested with collagenase A/D and DNase I, followed by passing through a 70 μm cell strainer and lysis of red blood cells. Intracellular staining or granyzme B (clone GB11), or TCF1 (clone S33-966) was performed on single cell suspensions of tumors using BD Cytofix/Cytoperm Plus Kit (Cat No.555028, BD Biosciences) according to the manufacturer's instructions.

ELISA

ELISA was performed using kits to detect mouse IFNβ (Cat No. 42400, PBL ASSAY SCIENCE), human IFNβ (Cat No. 41410, PBL ASSAY SCIENCE) human IL-12 p70 (Cat No. D1200, R&D Systems) and human TNFα (Cat No. 430204, Biolegend). All results (n=3) are expressed as the mean ± SEM.

ELISPOT analysis

Single cell suspensions from pooled mouse spleens were subjected to magnetic bead isolation of $CD8^+$ T cells according to manufacturer's instructions (Cat No.130-117-044, Miltenyi Biotec). Next, 3×10^5/well purified $CD8^+$ T cells and 1×10^5/well of 50Gy irradiated tumor cells were plated in triplicate wells and incubated in 96-well plates at 37°C for 24h. Tumor cells were stimulated with IFNγ (Cat No. 315-05, Peprotech) to increase MHC expression 1 day before coculture. T cells were also cultured alone or with Concavalin A as negative or positive controls, respectively. Plates were washed 6 times with PBS + 0.05% Tween 20 and 100 μl/well of biotinylated anti-IFNγ (Cat No. 13-7312-85, eBioscience) diluted to 1 μg/ml in PBS + 0.05% Tween 20 was added. Avidin-HRP (Cat No. 554058, BD Biosciences) was used as detection reagent. Spot counting was done using ImmunoSpot ELISpot plate reader (Cellular Technologies, Ltd). The release of IFNγ by T cells was normalized to ConA treatment–induced release of IFNγ in the same sample T cells.

Single cell RNA-sequencing (scRNA-seq)

scRNA-seq was performed using the 10X Genomics Chromium System (10X Genomics, Pleasanton, CA) by the Molecular Genomics Core at the Moffitt Cancer Center. B16-F10 tumor–bearing mice were injected with Ad-Null, Ad-MEM40, Ad-mIFNβ and the combination. Mice were cardiac-perfused with PBS containing 10 U/ml heparin to clear peripheral blood, and single cell suspensions were prepared by incubating minced tumor in 1 mg/ml collagenase A and 50 U/ml DNase I at 37°C for 20 min with agitation, followed by passing through a 70μm cell strainer and lysis of red blood cells for 2 min at room temperature. Each scRNA-seq sample was pooled from 3 different similarly treated tumors, $CD11c^+MHC\text{-}II^+$ sorted cells were sorted as in Supplementary Figure S2 by flow cytometry and then washed twice with 1X PBS (calcium and magnesium-free) containing 0.04% weight/volume BSA and resuspended in the same buffer following the cell preparation guide from 10x Genomics. The cell viability and counts were obtained by AO/PI dual fluorescent staining and visualization on the Nexcelom Cellometer K2 (Nexcelom Bioscience LLC, Lawrence, MA). Cells were then loaded onto the 10X Genomics Chromium Single Cell

Controller at a concentration of 1,000 cells/μl in order to encapsulate up to 10,000 cells per sample. Briefly, the single cells, reagents, and 10x Genomics gel beads were encapsulated into individual nanoliter-sized Gelbeads in Emulsion (GEMs) and then reverse transcription of poly-adenylated mRNA was performed inside each droplet at 53°C. The cDNA libraries were then completed in a single bulk reaction by following the 10X Genomics Chromium NextGEM Single Cell 3' Reagent Kit v3.1 user guide, and 50,000 sequencing reads per cell were generated on the Illumina NovaSeq 6000 instrument. Demultiplexing, barcode processing, alignment, and gene counting were performed using the 10X Genomics CellRanger v6.1.2 software, and analysis results were visualized using 10x Genomics Loupe browser v6.0.0.

scRNA-seq data processing, batch effect correction, and clustering.— Sequencing reads were mapped against mm10 mouse transcriptome and processed for unique molecular identifier (UMI) counting and barcodes filtering using Cell Ranger (v3.0, 10X Genomics). Barcodes with UMI counts passing threshold for cell detection were imported to Seurat v4.0 (48) for analysis. Cells with less than 200 genes detected or with greater than 10% mitochondrial UMIs were further filtered out; genes detected in less than three cells were excluded. Doublets were detected using Scrublet (49), doubletCells implemented in scran (50), DoubletFinder (51), and scDblFinder, assuming 0.08% doublet rate for every 1000 cells. Cells identified as doublets by at least two methods were removed. Raw UMI counts were then log-normalized and the top 4,000 variable genes were detected in each sample independently. S and G2/M cell cycle phase scores were assigned to cells using *CellCycleScoring* function. To remove batch effects between samples, samples were further integrated using *IntegrateData* function (52) in Seurat with parameter anchor.features =8000. Scaled z-scores for each gene were calculated using ScaleData regressing against total reads count, mitochondrial UMIs percentage, and cell cycle phases. Principal component analysis was performed on the integrated data and a shared nearest neighbor (SNN) graph was constructed based on the first 40 principal components. A total of 23 clusters were identified using the Louvain clustering (53) implemented in *FindClusters* function at resolution=0.8. Uniform manifold approximation and projection (UMAP) was used to visualize gene expression and clusters.

Differential gene expression analysis and cluster annotation.—Differential expression analysis for each cluster was performed using *FindAllMarkers* function in Seurat with default settings. Genes with Bonferroni-corrected p-value <0.05 and an average log-fold change > 0.25 were considered differentially expressed. Clusters were further annotated by comparing differential genes with markers previously associated with melanocytes (*Pmel*, *Mlana*), T cells (*Cd3e, Cd3d, Cd3g*), fibroblasts (*Col1a1*, *Col1a2*, *Nav1*), cDC1 (*Xcr1*, *Clec9a*, *Itgae*, *Batf3*), cDC2 (*Lilrb4a*, *Itgax*, *Csf1r, Mgl2*), mregDC (*Fscn1*, *Ccl22*, *Cacnb3*, *Ccr7*, *Fabp3*), pDC (*Siglech*, *Ccr9*, *Bst2*, *Pacsin1*, *Tcf4*), and proliferation (*Stmn1*, *Cdk1*, *Mki67*). For marker gene bubble plot, gene-level average expression was calculated for each cluster and then Z-score normalized.

In vitro human DC Stimulation

Healthy donor PBMCs were obtained from Florida Blood Services, purified by Ficoll spin separation of buffy coats followed by purification of $CD14^+$ cells (Cat no. 130-050-201, Miltenyi Biotec) and culturing in RPMI 1640 with 10% FBS with 10ng/ml GM-CSF and IL-4 (Cat No. 215-GM and 204-IL respectively, R&D Systems) for 6 days. On D5, A549 cells were infected with adenovirus at MOI=10 for 24h and then washed three times with PBS to remove free virus. On D6, monocyte-derived DCs (MoDCs) were plated at 1×10^6 per ml in serum free RPMI1640 and cocultured with adenovirus-infected A549 tumor cells for 48 hrs. Single cell suspensions were prepared and subjected to flow cytometry analysis or sorting for RNA-sequencing.

Bulk RNA-sequencing on Human DCs—Cells were gated on strict forward and side scatter parameters to ensure single-cell separation. In addition, the L/DNIR negative population was used for viable cells. The target cells were gated on HLA-DR^+CD11c^+ DCs derived from monocytes of 3 healthy donors by using FACSAira SORP housed in BioProtect IV BSC (BD Biosciences). Total RNA was extracted (QIAGEN called RNeasy Plant Mini Kit, Cat No. 74904) from human DCs after sorting HLA-DR^+CD11c^+ cells and RNA was then quantitated using the Qubit fluorometer (ThermoFisher Scientific, Waltham, MA) and screened for quality on the Agilent TapeStation 4200 (Agilent Technologies, Santa Clara, CA). The sequencing libraries were prepared using the Takara SMARTer Stranded Total RNA-seq Kit v2 Pico Input Mammalian kit (Takara Bio USA Inc., San Jose, CA) by the Molecular Genomics Core at the Moffitt Cancer Center. Briefly, 2ng of RNA was used to generate cDNA and a strand-specific library following the manufacturer's protocol. Library quality control steps were performed, including TapeStation size assessment and quantification using the Kapa Library Quantification Kit (Cat No. 07960298001) Roche, Wilmington, MA). The final libraries were normalized, denatured, and sequenced on the Illumina NextSeq 2000 sequencer with the P2-200 cycle reagent kit (Cat No. 20046812) to generate 60 million 105-base read pairs per sample (Illumina, Inc., San Diego, CA).

RNA-Seq Analysis: Paired-end RNA sequencing fastq files were aligned to the hs37d5 reference genome using the STAR aligner v2.5.3a. Expression counts were summarized at the gene level against the gencode v19 gene model using featurecounts v1.5.3. Read counts were normalized to library size estimates using the R package DESeq2 v1.20.0. Differential gene expression for treatment effects was done in DESeq2 using a paired design. The ranked gene list was used to perform pre-ranked gene set enrichment analysis (GSEA v4.0.2 (54)) to assess the enrichment of hallmarks, curated gene sets, and gene ontology (55) terms in MSigDB. The resulting normalized enrichment score (NES) and FDR controlled p-values were visualized in bar plot.

H&E, IHC staining and tumor quantification

Mouse tumors were directly fixed in 10% formalin in PBS and mouse lungs were insufflated with 10% formalin in PBS and fixed overnight. H&E and IHC were performed on fixed and paraffin-embedded samples. Tumors sections were cut on a microtome and stained according to standard protocols by Tissue Core, Moffitt Cancer Center. H&E and IHC (CD8 Cat No. 98941S, Cell Signaling Technologies) stained slides were scanned using an Aperio

AT2 digital pathology system (Leica Biosystems Inc., Vista, California) with a 20X 0.7NA objective lens. Whole slide H&E images were viewed with Aperio Imagescope software and regions of interest (ROIs) were annotated by an experienced digital pathology analyst to outline tumor regions. The total area of the tumor ROIs was calculated and normalized by total tissue area to determine the percent of tumor burden for each sample. The CD8 stained IHC images were imported into Definiens Tissue Studio v 4.7 (Definiens Inc., Munich, Germany) where a cell detection algorithm was used to enumerate $CD8^+$ and $CD8^-$ cells. The intensity threshold for positivity was set using the positive and negative staining controls as a guide. The $CD8^+$ cell counts were normalized by total cell number (% positive cells) and area (number of positive cells per mm^2). In some cases, heavy necrotic regions were manually omitted from the analysis to avoid false positive staining due to excessive tissue debris.

Human tumor ex vivo studies

Fresh deidentified lung cancer specimens were collected under an IRB-approved protocol (Advarra Inc.). Briefly, samples were obtained from 3 patients who provided written informed consent and who were undergoing standard of care surgical resection of lung cancer with excess tumor tissue beyond what was necessary for routine pathologic characterization (ideally at least 1cm × 1cm size). The studies were conducted in accordance with the Declaration of Helsinki. Freshly resected tumors were transported from the operating room to the pathology suite and initially stored in RPMI media. Tumor pieces were injected with PBS or 1×10^9 MEM-288 and cultured for 2 days. After a 20 min digestion with 2mg/ml collagenase A in 40ml DMEM + 80μl DNase (50 U/ml), single cell suspensions were processed and analyzed as described in the flow cytometry section. Tumor supernatants were used to determine levels of IFNβ by ELISA.

Human studies

A phase 1 trial was activated March 1, 2022, at the Moffitt Cancer Center in which single agent MEM-288 is administered by intratumoral injection in patients with advanced/metastatic cancer (ClinicalTrials.gov trial registration ID: NCT05076760). This part 1a study titled “Phase I Study of MEM-288 Oncolytic Virus in Solid Tumors including Non-Small Cell Lung Cancer (NSCLC)” is sponsored by Memgen, Inc and being conducted at 2 sites: Moffitt Cancer Center and Duke Cancer Institute. MEM-288 is administered as monotherapy to patients with advanced solid tumors, including NSCLC, refractory to standard therapies. Part 1a employs dose escalation using a BOIN design of 3 dose levels (1×10^{10}, 3.3×10^{10}, 1×10^{11} viral particles) with the primary objective to determine the maximum tolerated dose (MTD) of MEM-288. Eligibility criteria: patients (≥ 18 years old) with either advanced/metastatic NSCLC, cutaneous squamous-cell carcinoma (cSCC), Merkel cell, melanoma, triple negative breast cancer (TNBC), pancreatic cancer, or head and neck cancer, who progressed following previous anti-PD-1/PD-L1 therapy, with a tumor lesion which is accessible for injection. Intratumoral injection of MEM-288 is administered by a qualified Interventional Radiologist/Clinician to a palpable cutaneous/subcutaneous lesion, or under CT or ultrasound guidance of a percutaneously accessible tumor. Only one tumor lesion is injected per treatment. Injected tumor should be ≥ 1 cm^3 in volume and should not encase, or be adjacent to, vital neurovascular structures. Patients receive a

minimum of 2 and a maximum of 6 administrations of MEM-288. Tumor biopsies from the injected lesions are obtained at 2 timepoints: prior to first treatment and again at 3 weeks after initiation of treatment. For each tumor biopsy, 6 passes with 18–20-gauge needle are used to obtain tumor tissue before and after 1 MEM-288 injection. 3 passes are formalin-fixed and were used for mIF studies. The other 3 passes are snap frozen and used for generating nucleic acids (RNA and DNA). Serial peripheral blood collections are at screening and during treatment. PBMC DNA is used to determine systemic presence of potential tumor-reactive T cells by TCRβ sequencing using the ImmunoSEQ assay (see T-cell receptor beta chain sequencing (ImmunoSEQ assay)). The results reported herein are based on the first 2 enrolled patients, both NSCLC, and treated with 1×10^{10} MEM-288. In both patients, MEM-288 was injected in skin-palpable tumor lesions. The studies were conducted in accordance with the Declaration of Helsinki and performed after approval by an institutional review board (Advarra Inc.) and in accordance with an assurance filed with and approved by the U.S. Department of Health and Human Services. Informed written consent was obtained from each subject.

Multispectral Immunoflorescence (mIF)—FFPE tissue samples from biopsies of patients enrolled in the MEM-288 clinical trial were immunostained using the PerkinElmer OPAL ™ 7-Color Automation IHC kit (Cat No. NEL821001KT) on the BOND RX autostainer (Leica Biosystems, Vista, CA). The OPAL 7-color kit uses tyramide signal amplification (TSA)-conjugated to individual fluorophores to detect various targets within the multiplex assay. Sections were baked at 65^0C for one hour then transferred to the BOND RX (Leica Biosystems). All subsequent steps (e.g., deparaffinization, antigen retrieval) were performed using an automated OPAL IHC procedure (PerkinElmer). OPAL staining of each antigen occurred as follows: slides were blocked with PerkinElmer blocking buffer for 10 min then incubated with primary antibody at optimized concentrations followed by OPAL HRP polymer and one of the OPAL fluorophores. Primary antibodies used for mIF are listed in supplementary Table S1. Individual antibody complexes are stripped after each round of antigen detection. After the final stripping step, DAPI counterstain is applied to the multiplexed slide and is removed from BOND RX for coverslipping. Autofluorescence slides (negative control) were included, which use primary and secondary antibodies omitting the OPAL fluors and DAPI. All slides were imaged with the Vectra®3 Automated Quantitative Pathology Imaging System.

Quantitative Image Analysis:

Multi-layer TIFF images were exported from InForm (AKOYA) and loaded into HALO (Indica Labs, New Mexico) for quantitative image analysis. The tissue was segmented into individual cells using the DAPI marker which stains cell nuclei. For each marker, a positivity threshold within the nucleus or cytoplasm was determined per marker based on published staining patterns and intensity for that specific antibody. After setting a positive fluorescent threshold for each staining marker, the entire image set was analyzed with the created algorithm. The generated data includes positive cell counts for each fluorescent marker in cytoplasm or nucleus, and percent of cells positive for the marker. The markers shown are PCK, CD3, CD8, CD68, TCF1 and DAPI. These studies were performed in our Advanced

Analytical and Digital Pathology laboratory under the Pathology Department at Moffitt Cancer Center.

T-cell receptor beta (TCRβ) chain sequencing (ImmunoSEQ assay)—Genomic DNA of biopsy tissue or PBMCs was isolated using DNeasy Blood & Tissue Kit (Qiagen Cat No. 69506) according to manufacturer recommendations. TCR repertoire analysis was performed using the Adaptive Biotechnologies ImmunoSEQ assay v3. The CDR3 locus of sorted T cells were amplified by ImmunoSEQ hsTCRB kit (ImmunoSEQ hsTCRB kit v3 – Adaptive Biotechnologies Cat No. ISK10101) and sequenced on the Illumina NextSeq 500 to a targeted depth of 2 million sequencing reads per sample. The data were analyzed using the Adaptive Biotechnologies ImmunoSEQ Analyzer software, to identify the V, D, and J genes, filter non-productive sequences, and report and track T-cell clones. Productive clones and their frequencies were exported for further analysis. Shared clones between any tumors and any blood samples at both pre-treatment and on-treatment time points were visualized by R package eulerr. The proportional frequencies of top 10 most abundant clonotypes in tumors were tracked across all samples at all time points and visualized by *trackClonetypes* function in R package immunarch (56), where T cells with identical CDR3 amino acid sequence and V gene were considered as the same clonotype.

Statistical Analysis

Tumor-bearing mice were randomly assigned to the different treatment groups. Experimenters were not blinded to the treatment groups. In therapeutic studies with different treatments, 5–10 mice were used to have 80% power to detect a difference in tumor size of 50% between treatment and control groups with 95% confidence (41). 2-tailed Student's t-test with Welch's correction was used to determine significance of differences between samples as in previous studies (57). GraphPad Prism 6 software (GraphPad Software Inc.) was employed to determine significance: $P < 0.05$. *<0.05; **<0.01; ***<0.001. Relative tumor size difference between treatment groups was determined using two-way ANOVA followed by Tukey multiple comparison test. Survival differences were determined using Kaplan-Meier estimator method. P-value was calculated by Mantel-Cox test. Heatmap analysis of bulk RNA-seq data was performed through Morpheus software (Broad Institute, Cambridge, MA).

Data availability

RNA-seq data from 12 human DC samples is available in GEO (accession number GSE223342). scRNA-seq data from 4 mouse DC samples is available in GEO (accession number GSE223344). Human TCR sequences are available at ImmuneACCESS through the manuscript PMID. All other generated in this study are available within the article and its supplementary data files or from the corresponding author upon reasonable request.

Results

MEM40 and IFNβ trigger strong activation of tumor cDCs

Towards the goal of developing new therapeutic modalities, we investigated the impact of individual and combined activation of CD40 and type 1 IFN pathways on mouse tumor

cDCs. To this end, we utilized replication-deficient adenoviruses expressing a membrane-stable CD40L (MEM40) (39,40), mouse IFNβ (mIFNβ) and a control null virus (Ad-Null). *In vitro* studies showed that these viruses yielded robust expression of MEM40 and IFNβ (Supplementary Fig. S1). Mice bearing B16-F10 tumors were injected intratumorally on day 12 after s.c. tumor cell inoculation with $10e^9$ Ad-Null (NULL), $5\times10e^8$ Ad-Null + $5\times10e^8$ Ad-MEM40 (MEM40), $5\times10e^8$ Ad-Null + $5\times10e^8$ Ad-mIFNβ (mIFNβ) or $5\times10e^8$ Ad-MEM40 + $5\times10e^8$ Ad-mIFNβ (COMBO) infectious units (Fig. 1A). We evaluated an early treatment timepoint of 3 days after a single injection to determine the potential direct effects of MEM40 and IFNβ on cDCs in B16-F10 tumors. Both IFNβ and MEM40 + IFNβ, but not MEM40 alone, significantly reduced numbers of cDC1 ($CD11c^+$MHC-$II^+CD103^+CD11b^-$) and cDC2 ($CD11c^+$MHC-$II^+CD103^-CD11b^+$) (Fig. 1B, Supplementary Fig. S2, S3). The combined expression of MEM40 + IFNβ induced the largest increase in level of expression of the co-stimulatory molecules CD80 and CD86 and the lymph node homing receptor CCR7 in cDC1 (Fig. 1B–E). A similar but less significant stimulatory effect was seen in cDC2 (Supplementary Fig. S3). MHC-I expression also exhibited a trend towards increased expression in cDC1 and cDC2 after MEM40 + IFNβ treatment (Fig. 1F and Supplementary Fig. S3). These results suggest that MEM40 + IFNβ expression in the TME triggers upregulation of CD80 and CD86 co-stimulatory molecules and lymph node trafficking receptor CCR7.

To provide further insight into treatment impact on DCs, we sorted MHC-II^+CD11c^+ cells from tumors for scRNA-seq. The vast majority of MHC-II^+CD11c^+ cells were of the DC lineage, including cDC1, cDC2 and plasmacytoid DCs (pDCs) along with few contaminating fibroblasts and melanocytes (Fig. 1G). Clusters were annotated by comparing differential genes with markers previously associated with specific cell types (Fig. 1H and Supplementary Fig. S4). Sub-clusters combined into major cDC types showed that the strongest effect was in COMBO treated tumors, most notably a 6-fold expansion compared to Ad-Null treated tumors of DCs with gene expression profile of previously described for mregDCs (Fig. 1I, J) (29). The top differentially expressed genes (DEG) in these cells include *Ccr7* and *Ccl5* (Fig. 1H), as well as *Il12b*, *Cxcl9*, *Cd40*, *Cd80* and *Cd86* (Supplementary Table S2). mregDCs can be derived from cDC1 and cDC2 subsets and function as key drivers of T-cell activation in lymph nodes (29). Together with the flow cytometry results, these findings indicate that MEM40 + IFNβ activate cDCs to generate mature DCs with a high activation and migratory phenotype.

MEM40 + IFNβ promote tumor DC trafficking and activation in draining lymph nodes

We next determined treatment impact on cDC numbers and phenotype in tumor-draining inguinal lymph nodes. The main cDC1 types in lymph nodes are migratory $CD103^+$ and resident $CD8\alpha^+$ cDC1, besides the more numerous $CD11b^+$ cDC2 subset. MEM40 + IFNβ led to the highest proportion of the migratory $CD103^+$ cDC1 suggesting increased migration to lymph nodes (Supplementary Fig. S5 and S6A). In addition, combined MEM40 + IFNβ led to the highest expression of co-stimulatory markers CD80 and CD86 by cDC1 and cDC2 (Supplementary Fig. S6B).

To further investigate the treatment impact on DCs, we determined whether the reduction in numbers of cDC1 in tumors was due to their migration to the draining lymph nodes. As CCR7 deficiency impairs cDC1 lymph node trafficking (20), we compared the effect of Ad-Null control virus and COMBO viruses in WT and CCR7$^{-/-}$ mice. While COMBO treatment reduced the numbers of cDC1 and cDC2 in tumors in WT mice, no similar reduction was seen in CCR7$^{-/-}$ mice (Fig. 2A). Furthermore, migratory CD103^{+} cDC1 were virtually absent in draining lymph node in CCR7$^{-/-}$ mice and this did not change after COMBO treatment (Fig. 2B). Lymph node resident CD8α^{+} cDC1 numbers were also substantially lower in CCR7$^{-/-}$ mice whereas cDC2 numbers were reduced to a lesser extent, suggestive of just partial dependence on CCR7 (Fig. 2B). These results suggest that reduction in the number of intra-tumoral cDC1 after COMBO treatment is likely due to their trafficking to lymph nodes.

To directly test impact on DC migration, we used Zs-Green expressing B16-F10 (20) (Fig. 2C). This stable fluorophore antigen resists lysosomal degradation and allows detection of tumor antigen uptake in lymph node DCs (20). While COMBO treatment triggered a reduction in the number of cDCs in tumors, a similar percentage of Zs-Green^{+} cDC1 and cDC2 was seen in tumors suggesting that treatment did not increase antigen uptake (Fig. 2D, E). Furthermore, both Zs-Green^{+} and Zs-Green^{-} tumor cDC displayed an upregulation of activation marker expression after the COMBO treatment (Supplementary Fig. S7). Conversely in lymph nodes, we observed a 2–3-fold increase in percentage of Zs-Green^{+} total DCs, migratory CD103^{+} cDC1, cDC2, as well as resident CD8α^{+} cDC1 after the COMBO treatment (Fig. 2F–I). Tumor antigen acquisition by CD8α^{+} cDC1 is consistent with previous studies showing antigen “hand-over” by migratory CD103^{+} cDC1s to this lymph node resident population (20). Both Zs-Green^{+} and Zs-Green^{-} lymph node DCs had increased activation marker expression after COMBO treatment, but Zs-Green^{+} DCs tended to have higher expression after COMBO treatment (Supplementary Fig. S8). Collectively, these results demonstrate that the COMBO treatment triggers strong cDC trafficking and antigen transport to draining lymph nodes, concomitant with acquisition of a robust activation phenotype in all major lymph node cDC subsets.

FDA approved OVs (T-VEC) and several OVs in development rely on expression of encoded GM-CSF to increase DC levels and TME immune activation (58–60). However, to our knowledge, previous studies have not investigated localized and systemic effects of *in situ* GM-CSF administration versus bona fide CD40/type 1 IFN DC activators. Using GM-CSF expressing adenovirus (Ad-GMCSF) (Supplementary Fig. S9A), a significant increase in cDC2 but not cDC1 was observed after intratumor injection (Supplementary Fig. S9B). However, unlike the stimulatory effect of COMBO, GM-CSF did not induce tumor cDC activation and had no stimulatory effect on DC migration to LNs (Supplementary Fig. S9C–E). These results indicate that tumor CD40 and type 1 IFN pathway activation induce a superior DC response than GM-CSF.

Distinct and synergistic impact of MEM40 and IFNβ on human DC activation markers

We next determined the impact of MEM40 and IFNβ on normal human donor monocyte-derived DCs (Mo-DCs) phenotype. We used an experimental design where human A549

lung cancer cells were first infected with Ad-Null or adenoviruses expressing human IFNβ, MEM40 or MEM40 + IFNβ for 24h followed by removal of virus-containing supernatant and co-culture with Mo-DCs for 48h (Fig. 3A). While both MEM40 and IFNβ individually increased CD80, CD86, CCR7 and MHC-I (HLA-B) expression, the highest increase in these markers was evident in MEM40 + IFNβ treated human DCs (Fig. 3B). We also observed that MEM40 expression dramatically reduced CD40 levels, possibly through ligand-induced receptor internalization, but IFNβ allowed retention of CD40 expression (Fig. 3B), which could serve to sustain CD40 signaling. MEM40 alone, but not IFNβ, increased expression of Th1-promoting cytokines IL12-p70 and TNFα (Fig. 3C, D). As seen with cell surface markers, the combination of MEM40 + IFNβ also led to the highest expression of these cytokines. Consistent with the mouse studies, these results indicate that combined MEM40 + IFNβ expression induced the highest-level activation of human DCs.

To define the individual and combined effects of MEM40 and IFNβ on human DC gene expression, we used the experimental design in Fig. 3A followed by sorting of MHC-II^+CD11c^+ cells for bulk RNA-sequencing. DCs were derived from 3 independent healthy donors. Both MEM40 and IFNβ induced significant change in expression of a substantial subset of genes (Supplementary Table S3). Within the top ~80 named genes induced by the COMBO treatment, we found that MEM40 and IFNβ enhanced expression of distinct target genes (Fig. 3E). We next determined impact on genes associated with DC functionality. Genes engaged in the MHC-I antigen presentation pathway, *HLA-A, HLA-B, HLA-C, B2M, TAP1* and *TAP2,* were induced more strongly by IFNβ than by MEM40 (Fig. 3F). On the other hand, key DC activation–associated genes *CD80*, *CD86*, *CD40*, *CCR7, IL12A*, *IL12B* and *IL23A* were induced by both MEM40 and IFNβ, but more strongly by MEM40 (Fig. 3F). Hallmark Pathway analysis revealed an increase in both NF-κB (TNFA-NF-κB) and IFN pathways by MEM40 and IFNβ (Fig. 3G); however, as expected, analysis of COMBO vs. individual treatment demonstrated that MEM40 contributed to NF-κB activation while IFNβ contributed to IFN pathways activation in the COMBO samples (Supplementary Fig. S10). Collectively, these results indicated that target gene expression and pathway activation in the COMBO treatment was due to individual effects of MEM40 and IFNβ while for key DC functionality genes both MEM40 and IFNβ could independently induce expression.

Combined CD40 and type 1 IFN pathway activation in the TME promotes systemic antitumor T-cell responses

We next determined whether cDC activation by MEM40 and IFNβ impacted the antitumor T-cell response. For these studies, we used a different timeline than the above 3-day treatments to allow sufficient time for development of an initial T-cell response. As multiple intralesional injections are not feasible for most cancer patients, we determined treatment efficacy after 2 virus injections administered 4 days apart. The analyses below were performed 7 days after the second virus injection (i.e., 23 days after tumor cell injection and 11 days after treatment initiation). Tumor growth until day 23 showed that while both MEM40 and IFNβ reduced tumor growth compared to Ad-Null, the most significant reduction in tumor growth was observed with the COMBO treatment (Fig. 4A). No effect on tumor growth was observed with Ad-Null compared to untreated controls. Furthermore, the COMBO treatment resulted in significantly reduced tumor growth compared to the

individual MEM40 and IFNβ treatments. Day 23 tumors were then used to characterize the intratumoral lymphoid and myeloid cell types by flow cytometry. Compared to Ad-Null injected tumors, $CD8^+$ T cells were significantly increased by ~3-fold in COMBO injected tumors (Fig. 4B). $CD4^+$ T cells, B cells, macrophages and neutrophils were not significantly impacted by treatment vs. Null control arm (Supplementary Fig. S11). Notably, cDC1, but not cDC2, showed a significant reduction in numbers after MEM40, IFNβ and COMBO treatment in comparison to Ad-Null treatment (Fig. 4C, D). This was different than at the day 3 timepoint (Fig. 1B and Supplementary Fig. S3), as cDC1 numbers were also reduced by MEM40, suggesting different kinetics of impact of these transgenes with IFNβ dominating at early timepoints. A possible explanation is that IFNβ, being a diffusible mediator of DC activation, may act more rapidly within the TME while CD40 activation requires cell-to-cell interactions between adenovirus-infected MEM40-expressing cells and tumor DCs, which is likely to be a temporally slower process. Within the intratumoral $CD8^+$ T-cell population, we noted an increase in $TCF1^+$ $CD8^+$ T cells as well as Granzyme B^+ $CD8^+$ T cells in murine studies, indicating that the COMBO treatment enhanced both stem-like and effector T cells (Supplementary Fig. S11G–H). To determine whether intralesional virus injections led to a systemic increase in tumor-reactive $CD8^+$ T cells, we performed IFNγ ELISPOT assays with splenic $CD8^+$ T cells. Both Ad-MEM40 and Ad-mIFNβ significantly increased the number of tumor-antigen reactive T cells compared to Ad-Null, but the highest increase was observed after COMBO treatment (Fig. 4E; also see Supplementary Fig. S12A for additional assay information), consistent with the delay in tumor growth. These differences were observed in both ConA normalized (Fig. 4E) and non-normalized results (Supplementary Fig. S12A). Notably, consistent with lack of localized DC stimulatory effect of GM-CSF, Ad-GM-CSF administration did not activate a systemic antitumor T-cell response (Supplementary Fig. S9F).

To confirm antitumor activity in a different tumor model, we used the transplantable 344SQ model derived from a KRAS-G12D/TP53 (KP) mutant lung tumor (61). 344SQ tumor inoculation at the s.c. site results in metastasis to multiple sites, including lungs (61), which can be controlled by high level T-cell activation (62). As with B16-F10 tumors, 344SQ tumors were injected IT on D12 and 16 with viruses following which we monitored s.c. tumor growth and numbers of lung metastases. Similar to B16-F10, we observed significant growth reduction after Ad-MEM40 and Ad-mIFNβ injection with the most significant reduction after the COMBO treatment (Fig. 4F). The COMBO treatment also resulted in significantly reduced tumor growth compared to the individual MEM40 and IFNβ treatments. Notably, these treatments significantly reduced lung metastases with the greatest reduction after the COMBO treatment (Fig. 4G, H). Furthermore, ELISPOT assays with splenic $CD8^+$ T cells showed a significant increase in tumor antigen reactivity with Ad-MEM40, Ad-mIFNβ and the highest elevation in the COMBO treatment (Fig. 4I). Together with above findings, these results suggest that cDC activation by MEM40 and IFNβ empowers systemic T-cell responses to control tumor growth.

Impact of CD40 and IFNAR1 absence on MEM40 and IFNβ induced T-cell responses

While both CD40 and type 1 IFNs are crucial for generation of antitumor T-cell responses, it is not clear whether they participate in the same or independent pathways to drive

$CD8^+$ T-cell cross-priming. To investigate this, we determined the impact of MEM40 and IFNβ on T-cell priming in mice lacking either CD40 or the IFNα/β receptor IFNAR1. Consistent with previous studies, no major developmental abnormalities in DC subsets in tumor and lymph nodes were noted in $CD40^{-/-}$ and $IFNAR1^{-/-}$ mice (19,36). While the MEM40-induced systemic T-cell response was eliminated in $CD40^{-/-}$ mice, it was only slightly reduced in $IFNAR1^{-/-}$ mice (Fig. 4J). Conversely, T-cell priming by IFNβ was eliminated in $IFNAR1^{-/-}$ mice but was unaffected in $CD40^{-/-}$ mice (Fig. 4J). Furthermore, T-cell priming by the COMBO treatment was only partially reduced in both the $CD40^{-/-}$ and the $IFNAR1^{-/-}$ mice (Fig. 4K). These findings suggest that CD40L and IFNβ stimulate T-cell priming independently of each other, explaining why the combination of these 2 agents leads to the highest level of T-cell activation. A key target of both CD40 and type I IFNs are cDC1 (34,36). Using $BATF3^{-/-}$ mice, which lack cDC1, we found that T-cell priming was eradicated after MEM40 and IFNβ expression, indicating a crucial role for this cDC subtype (Fig. 4L). After the COMBO treatment, small residual priming activity was observed, suggesting that other DC or APC subsets may play a role in T-cell priming (Fig. 4M).

Combination of MEM40 + IFNβ and ICIs enhances distant anti-tumor response

While our studies indicate that tumor activation of CD40 and type 1 IFN pathways promotes generation of tumor-reactive T cells, immune checkpoints such as PD-1 and CTLA-4 could dampen this response in both tumor and periphery. To test this, mice bearing B16-F10 primary tumors subjected to injection with viruses and non-injected contralateral (abscopal) tumors were treated systemically (intraperitoneal) with murine anti-PD-1/CTLA4 (Fig. 5A). Anti-PD-1/CTLA4 combination was only moderately effective against established B16-F10 tumors (Fig. 5B). While the COMBO virus treatment was more effective than anti-PD-1/CTLA4, COMBO + anti-PD-1/CTLA4 led to the most significant reduction in tumor growth (Fig. 5B). Notably, COMBO + anti-PD-1/CTLA4 also led to the most significant reduction in contralateral tumor growth (Fig. 5C) and resulted in the most significant increase in mouse overall survival (Fig. 5D). A similar strategy was employed in the 344SQ model. Treatment with COMBO + anti-PD-1/CTLA4 led to the most significant decrease in s.c. tumor growth while anti-PD-1/CTLA4 was minimally effective (Fig. 5E). Notably, lungs of mice revealed an essentially complete absence of metastases after COMBO + anti-PD-1/CTLA4 treatment (Fig. 5F). These results demonstrate that in 2 tumor models with minimal sensitivity to ICI, pairing COMBO with ICI treatment led to enhancement of efficacy against distant lesions.

Generation and in vivo testing of MEM-288 oncolytic adenovirus

The replication-deficient adenoviruses used above do not cause virus-mediated lysis of either mouse or human tumor cells. Furthermore, unlike human cells, mouse cells do not efficiently support wild-type or oncolytic adenovirus replication (63). OVs are designed for replication-induced oncolysis of cancer cells and tumor antigen release (7). We hypothesized that OV-induced tumor antigen release could synergize with MEM40 + IFNβ in amplifying antitumor T-cell responses. Towards the goal of clinical testing of the impact of MEM40 + IFNβ in cancer patients, we utilized a type 5 adenovirus backbone with an E1A Δ24 deletion that prevents Rb inactivation to allow replication and lysis of cancer cells but not

normal cells (43). This oncolytic adenovirus backbone was engineered to express MEM40 and human IFNβ and was designated as MEM-288 (Fig. 6A). As control, we used E1A Δ24 adenovirus that expresses GFP (Ad-GFP).

Infection of mouse B16-F10, 344SQ and human A549 lung cancer cell line with MEM-288, but not Ad-GFP, led to high-level secretion of IFNβ into the culture supernatant (Fig. 6B). In addition, infection of these cell lines with MEM-288 induced high MEM40 expression while infection with Ad-GFP led to high GFP expression (Fig. 6C). Notably, MEM-288 injection in freshly resected human NSCLC tumors induced IFNβ expression and MEM40 expression, especially in the $CD45^-$ population enriched in cancer cells (Fig. 6D, E). Neither Ad-GFP nor MEM-288 induced lysis of mouse B16-F10 and 344SQ (Supplementary Fig. S13). Adenovirus replication and ensuing cell lysis is relatively resistant to type 1 IFN (42). In fact, compared to Ad-GFP, we observed stronger oncolysis by MEM-288 in A549 cells *in vitro* (Fig. 6F) as well as in A549 tumors *in vivo* (Fig. 6G).

We next determined the *in vivo* activity of MEM-288 in the B16-F10 and 344SQ tumor models. Since MEM-288 expresses human IFNβ, we first determined the ability of human IFNβ to induce antitumor T-cell responses using the B16-F10 model. Previous studies have shown that human IFNβ has substantially lower activity in mice but that it can induce signaling in the mouse immune compartment (64). Unlike mouse IFNβ, human IFNβ expressed by a replication-deficient adenovirus did not enhance a T-cell response (Fig. 6H). However, the combination of human IFNβ and MEM40 significantly enhanced the T-cell response compared to MEM40 alone (Fig. 6H) suggesting that residual human IFNβ activity may be sufficient to enhance CD40 signaling response. Consistently, in comparison with Ad-GFP, MEM-288 induced a greater antitumor response as well as T-cell activation in B16-F10 (Fig. 6I, J). Since these viruses are not oncolytic in mouse cells, the observed antitumor responses are likely due to immune stimulatory effect of the products encoded by the transgenes. To confirm replication-deficient virus findings with MEM-288, we determined the effect of tumor injection of MEM-288 on the growth of injected and non-injected contralateral B16-F10 tumors and synergy with ICI treatment. The combination of anti-CTLA4 + anti-PD-1 and MEM-288 significantly reduced growth of both injected and contralateral tumors compared to individual treatments and significantly increased mouse survival (Fig. 6K–M). In addition, as observed with replication-deficient viruses in the 344SQ model, MEM-288 led to a significant decrease in injected tumor growth and lung metastasis (Fig. 6N, O). $CD8^+$ IHC further revealed significantly higher TIL density in lung metastases of MEM-288 treated mice (Fig. 6P). Together, these results demonstrate single-agent antitumor activity of MEM-288 that was enhanced when combined with ICIs.

MEM-288 modulation of the TME and systemic T-cell immunity in NSCLC

We initiated a first-in-human Phase 1A dose-escalation study of MEM-288 in multiple solid tumors, including melanoma and NSCLC, with the primary objective to determine the safety and maximum tolerated dose (NCT05076760). Biopsy tissues from the first 2 enrolled patients, both NSCLC, were used to determine MEM-288 impact on the TME. 3 tumor biopsy passes were used to sample the tumor prior to MEM-288 injection (pre-treatment biopsy) followed by 3 passes 21 days after the first biopsy (on-treatment biopsy),

which were used for mIF (Fig. 7A–D). mIF was conducted separately on each pass after pathological confirmation of integrity of FFPE tissue H&E slides. Palpable or accessible tumors for imaging-guided injections were used to administer MEM-288 without preference for the orthotopic tumor site. We detected a significant reduction in the percentage and density of PCK^+ malignant cells (Fig. 7A, B, E, F and Supplementary Fig. S14). Patient 2 had pronounced loss of viable tumor tissue after treatment resulting in higher variability in biopsy passes from different tumor areas. Statistically significant findings were therefore only obtained from patient 1 biopsy studies. These results mirrored clinical measurements of injected tumors that showed significant radiographic tumor shrinkage of −53% (patient 1) and −31% (patient 2) on day 22 after 1 MEM-288 injection. In addition, we saw a significant increase in percentage of $CD3^+$ T cells but not $CD68^+$ macrophages (Fig. 7A, B, G, H and Supplementary Fig. S14). We also saw a significant increase in percentage of $TCF1^+$ stem-like $CD8^+$ T cells (Fig. 7C, D, I, J and Supplementary Fig. S14). We surmise that MEM-288 can induce substantial remodeling of the TME most notably evident by increased numbers of T cells and especially stem-like T-cell subsets that are known to be associated with disease control (65–72).

Patient 1 biopsies and blood draws were used for TCRβ sequencing. The combined T clonotypes in all 3 tumor passes were increased from 1,497 in pre-treatment to 3,918 in on-treatment biopsies (Fig. 7K, L) indicating that MEM-288 likely increased the number of tumor antigen–specific T-cell clonotypes. In addition, shared clonotypes between tumor and blood increased from 922 to 1691 (Fig. 7K, L). Tracking the top-10 tumor clonotypes (top-10 highest total abundance in all pre- and on-treatment biopsies) in blood revealed a substantial increase that peaked on day 22 after MEM-288 treatment initiation (Fig. 7M). These results suggest that MEM-288 increases T-cell numbers and clonotype diversity leading to an increase in potential tumor-reactive T cells in the peripheral blood.

Discussion

In this study, we show that combined activation of CD40 and type 1 IFN pathways in the TME can strongly stimulate systemic antitumor $CD8^+$ T-cell responses through robust activation of DCs. When combined with ICI, MEM40 + IFNβ induced a potent abscopal tumor response indicating that this strategy can be effective against disseminated disease. For clinical translation of this approach, we developed an oncolytic virus (MEM-288) that expresses MEM40 and human IFNβ. Our clinical findings indicate that intratumoral MEM-288 administration in NSCLC patients was associated with loss of cancer cells, and increase in overall T cells and an increase in $CD8^+$ stem-like T cells, which are known to be associated with clinical benefit from ICI treatment and adoptive cell therapy (65–71). Furthermore, MEM-288 administration increased the systemic presence of tumor T-cell clonotypes. These studies provide strong rationale for further development of MEM-288 as a single-agent treatment and in combination with ICIs.

Our preclinical results indicate that the combination of MEM40 and IFNβ led to the highest levels of cDC1 and cDC2 activation and induction of systemic T-cell immunity. A striking effect of this treatment was the reduction in the number of tumor DCs and increase in trafficking to draining lymph nodes, which we believe is crucial for the mechanism of

action of this combination. Unlike the strong DC stimulatory effect of CD40 and type 1 IFN pathways, we found that GM-CSF expression did not increase DC activation, LN trafficking and had no effect on the systemic T-cell responses. As GM-CSF is widely used in OVs, our results suggest that OVs with strong activators of DCs are likely to be more therapeutically effective than those encoding GM-CSF. Furthermore, our results also demonstrate that strong activation of either CD40 or type 1 IFN can bypass the need for the other in T-cell activation. Thus, IFNβ induced T-cell priming was impaired in IFNAR1$^{-/-}$ but undiminished in CD40$^{-/-}$ mice. Conversely, MEM40 retained substantial T-cell priming activity in IFNAR1$^{-/-}$ mice but was abrogated in CD40$^{-/-}$ mice. While roles of CD40 and type 1 IFN pathways in cDC activation are established, their ability to act in an independent manner to stimulate T-cell priming helps explain why their dual activation induces the most potent cDC and T-cell activation. It is likely that these two activators provide specific inputs to DCs, e.g., CD40 may specifically control DC survival (73), which remain to be fully defined and likely impact T-cell responses in different ways. Our studies with human Mo-DC also showed that both MEM40 and IFNβ can upregulate key DC genes that regulate MHC-I antigen presentation and co-stimulation. However, the highest cell surface expression of MHC-I and co-stimulation markers in human DCs was observed with the MEM40 and IFNβ combination while in mice the combination also led to the highest levels of mregDC. Although both MEM40 and IFNβ enhanced antigen presentation and co-stimulation, they were also capable of inducing expression of unique transcriptomes that will likely impact DC functionality and the TME through mechanisms that remain to be defined. Analogous to the use of multiple therapeutics to maximize T-cell functionality (e.g., anti-PD-1 combined with anti-CTLA4 or LAG3), our results indicate that multimodal DC activation by MEM40 and IFNβ has strong potential to elicit robust antitumor T-cell immunity in cancer patients.

We believe our virus-based approach has significant advantages over strategies currently being tested to enhance CD40 and type 1 IFN signaling. While recent studies in pancreatic cancer have shown a promising response rate of combination of a systemically delivered CD40 agonistic antibody with ICI and chemotherapy, this was also associated with significant toxicity (74). Indeed, toxicity associated with systemic CD40 agonists has hindered approval of this otherwise promising therapeutic modality and consequently, approaches that induce more targeted CD40 activation are being developed (34,75). We believe that intratumoral administration, combined with the unique stable cell surface expression of recombinant CD40L (MEM40) in MEM-288 will limit systemic CD40 activation and thus provide patient benefit without significant toxicity. Indeed, in MEM-288 patients treated to date, we have not observed any dose limiting toxicity (DLT). Strategies to stimulate innate immunity by type 1 IFN expression have also been clinically tested through IT injection of STING and TLR9 agonists (5,6). TLR9 agonists have shown a promising response rate in ICI refractory melanoma, and this was associated with induction of type I IFN expression (5,76). However, the relatively labile nature of these agents can require repeat intratumoral injections (e.g., a median of 8 injections) (76), making their use in cancer patients who do not have superficial lesions more challenging. We believe that IFNβ expression by OVs can provide a superior approach for sustained activation of type 1 IFN signaling, which may therefore require fewer administrations. Sustained and combined

MEM40 + IFNβ expression by MEM-288 should therefore provide a superior signal for stimulating antitumor immunity than use of individual activators of these pathways currently being tested. To our knowledge, therapeutic approaches that combine activation of these two key pathways have not been tested in cancer patients.

We recently initiated a first-in-human Phase 1A dose-escalation study of MEM-288 in multiple solid tumors, including NSCLC. Studies of patient biopsies showed increase in T cells after treatment with MEM-288, replicating our murine studies. Notably, increase in $TCF1^+$ stem-like $CD8^+$ T cells after MEM-288 administration may be especially significant as this population is strongly associated with immunotherapy benefit (65–71). Previous studies have shown that presence of shared T-cell clonotypes in tumor and blood is associated with ICI benefit (77–84). In the first MEM-288 treated patient, we performed TCR sequencing on biopsy tissue and PBMCs. We found that after a single MEM-288 injection, shared clonotypes between tumor and blood were substantially increased and was especially notable when the top-10 tumor clonotypes were tracked in peripheral blood. Both the TME mIF and T-cell clonotype findings however need to be extended to additional NSCLC patients as well as patients with other tumor types before firm conclusions can be drawn on MEM-288 treatment impact on local and systemic responses. Nonetheless, if these changes after MEM-288 administration are confirmed, it would indicate that combining MEM-288 and ICIs has potential to increase patient benefit compared to ICIs alone.

Supplementary Material

Refer to Web version on PubMed Central for supplementary material.

Acknowledgments

We thank Moffitt colleagues Drs. Jose Conejo Garcia-Sastre, Daniel Abate-Daga and Shari Pilon-Thomas for helpful discussions on this work. We also thank Zhihua Chen for help with RNA-sequencing analysis, Chase D. Powell for help with human lung tumor studies, Wenjie Dai and Margaret Barlow for technical assistance, and Jonathan Nguyen and Carlos Moran Segura for assistance with mIF studies. These studies were supported by funds to AAB from Miles for Moffitt, Moffitt Foundation, Moffitt Lung Cancer Center of Excellence, Memgen Inc and NIH 5P50CA168536. We would like to acknowledge the Molecular Genomics, Cancer Informatics, Tissue Core, Analytic Microscopy, Advanced Analytical and Digital Pathology and Flow Cytometry shared facilities at Moffitt Cancer Center; an NCI designated Comprehensive Cancer Center supported by NIH P30-CA076292.

Funding information:

These studies were supported by funds to AAB from Miles for Moffitt, Moffitt Foundation, Moffitt Lung Cancer Center of Excellence, Memgen Inc and NIH 5P50CA168536. We would like to acknowledge the Molecular Genomics, Cancer Informatics, Tissue Core, Analytic Microscopy, Advanced Analytical and Digital Pathology and Flow Cytometry shared facilities at Moffitt Cancer Center; an NCI designated Comprehensive Cancer Center supported by NIH P30-CA076292.

References

1. Chen DS, Mellman I. Elements of cancer immunity and the cancer-immune set point. Nature 2017;541(7637):321–30 doi 10.1038/nature21349. [PubMed: 28102259]
2. Herbst RS, Soria JC, Kowanetz M, Fine GD, Hamid O, Gordon MS, et al. Predictive correlates of response to the anti-PD-L1 antibody MPDL3280A in cancer patients. Nature 2014;515(7528):563–7 doi 10.1038/nature14011. [PubMed: 25428504]
3. Joyce JA, Fearon DT. T cell exclusion, immune privilege, and the tumor microenvironment. Science 2015;348(6230):74–80 doi 10.1126/science.aaa6204. [PubMed: 25838376]

4. Tumeh PC, Harview CL, Yearley JH, Shintaku IP, Taylor EJ, Robert L, et al. PD-1 blockade induces responses by inhibiting adaptive immune resistance. Nature 2014;515(7528):568–71 doi 10.1038/nature13954. [PubMed: 25428505]
5. Ribas A, Medina T, Kummar S, Amin A, Kalbasi A, Drabick JJ, et al. SD-101 in Combination with Pembrolizumab in Advanced Melanoma: Results of a Phase Ib, Multicenter Study. Cancer discovery 2018;8(10):1250–7 doi 10.1158/2159-8290.CD-18-0280. [PubMed: 30154193]
6. Flood BA, Higgs EF, Li S, Luke JJ, Gajewski TF. STING pathway agonism as a cancer therapeutic. Immunological reviews 2019;290(1):24–38 doi 10.1111/imr.12765. [PubMed: 31355488]
7. Bommareddy PK, Shettigar M, Kaufman HL. Integrating oncolytic viruses in combination cancer immunotherapy. Nature reviews Immunology 2018;18(8):498–513 doi 10.1038/s41577-018-0014-6.
8. Seymour LW, Fisher KD. Oncolytic viruses: finally delivering. British journal of cancer 2016;114(4):357–61 doi 10.1038/bjc.2015.481. [PubMed: 26766734]
9. Bommareddy PK, Silk AW, Kaufman HL. Intratumoral Approaches for the Treatment of Melanoma. Cancer J 2017;23(1):40–7 doi 10.1097/PPO.0000000000000234. [PubMed: 28114253]
10. Wculek SK, Cueto FJ, Mujal AM, Melero I, Krummel MF, Sancho D. Dendritic cells in cancer immunology and immunotherapy. Nature reviews Immunology 2020;20(1):7–24 doi 10.1038/s41577-019-0210-z.
11. Andtbacka RH, Kaufman HL, Collichio F, Amatruda T, Senzer N, Chesney J, et al. Talimogene Laherparepvec Improves Durable Response Rate in Patients With Advanced Melanoma. J Clin Oncol 2015;33(25):2780–8 doi 10.1200/JCO.2014.58.3377. [PubMed: 26014293]
12. Dummer R, Gyorki DE, Hyngstrom J, Berger AC, Conry R, Demidov L, et al. Neoadjuvant talimogene laherparepvec plus surgery versus surgery alone for resectable stage IIIB-IVM1a melanoma: a randomized, open-label, phase 2 trial. Nature medicine 2021;27(10):1789–96 doi 10.1038/s41591-021-01510-7.
13. Dummer R, Hoeller C, Gruter IP, Michielin O. Combining talimogene laherparepvec with immunotherapies in melanoma and other solid tumors. Cancer Immunol Immunother 2017;66(6):683–95 doi 10.1007/s00262-017-1967-1. [PubMed: 28238174]
14. Ribas A, Dummer R, Puzanov I, VanderWalde A, Andtbacka RHI, Michielin O, et al. Oncolytic Virotherapy Promotes Intratumoral T Cell Infiltration and Improves Anti-PD-1 Immunotherapy. Cell 2018;174(4):1031–2 doi 10.1016/j.cell.2018.07.035. [PubMed: 30096300]
15. Malvehy J, Samoylenko I, Schadendorf D, Gutzmer R, Grob JJ, Sacco JJ, et al. Talimogene laherparepvec upregulates immune-cell populations in non-injected lesions: findings from a phase II, multicenter, open-label study in patients with stage IIIB-IVM1c melanoma. J Immunother Cancer 2021;9(3) doi 10.1136/jitc-2020-001621.
16. Ribas A, Dummer R, Puzanov I, VanderWalde A, Andtbacka RHI, Michielin O, et al. Oncolytic Virotherapy Promotes Intratumoral T Cell Infiltration and Improves Anti-PD-1 Immunotherapy. Cell 2017;170(6):1109–19 e10 doi 10.1016/j.cell.2017.08.027. [PubMed: 28886381]
17. Thorn M, Guha P, Cunetta M, Espat NJ, Miller G, Junghans RP, et al. Tumor-associated GM-CSF overexpression induces immunoinhibitory molecules via STAT3 in myeloid-suppressor cells infiltrating liver metastases. Cancer Gene Ther 2016;23(6):188–98 doi 10.1038/cgt.2016.19. [PubMed: 27199222]
18. Noubade R, Majri-Morrison S, Tarbell KV. Beyond cDC1: Emerging Roles of DC Crosstalk in Cancer Immunity. Front Immunol 2019;10:1014 doi 10.3389/fimmu.2019.01014. [PubMed: 31143179]
19. Ferris ST, Durai V, Wu R, Theisen DJ, Ward JP, Bern MD, et al. cDC1 prime and are licensed by CD4(+) T cells to induce anti-tumour immunity. Nature 2020;584(7822):624–9 doi 10.1038/s41586-020-2611-3. [PubMed: 32788723]
20. Roberts EW, Broz ML, Binnewies M, Headley MB, Nelson AE, Wolf DM, et al. Critical Role for CD103(+)/CD141(+) Dendritic Cells Bearing CCR7 for Tumor Antigen Trafficking and Priming of T Cell Immunity in Melanoma. Cancer cell 2016;30(2):324–36 doi 10.1016/j.ccell.2016.06.003. [PubMed: 27424807]
21. Salmon H, Idoyaga J, Rahman A, Leboeuf M, Remark R, Jordan S, et al. Expansion and Activation of CD103(+) Dendritic Cell Progenitors at the Tumor Site Enhances Tumor

Responses to Therapeutic PD-L1 and BRAF Inhibition. Immunity 2016;44(4):924–38 doi 10.1016/j.immuni.2016.03.012. [PubMed: 27096321]

22. Spranger S, Dai D, Horton B, Gajewski TF. Tumor-Residing Batf3 Dendritic Cells Are Required for Effector T Cell Trafficking and Adoptive T Cell Therapy. Cancer cell 2017;31(5):711–23 e4 doi 10.1016/j.ccell.2017.04.003. [PubMed: 28486109]
23. Duong E, Fessenden TB, Lutz E, Dinter T, Yim L, Blatt S, et al. Type I interferon activates MHC class I-dressed CD11b(+) conventional dendritic cells to promote protective anti-tumor CD8(+) T cell immunity. Immunity 2022;55(2):308–23 e9 doi 10.1016/j.immuni.2021.10.020. [PubMed: 34800368]
24. Gardner A, de Mingo Pulido A, Ruffell B. Dendritic Cells and Their Role in Immunotherapy. Front Immunol 2020;11:924 doi 10.3389/fimmu.2020.00924. [PubMed: 32508825]
25. Gardner A, Ruffell B. Dendritic Cells and Cancer Immunity. Trends Immunol 2016;37(12):855–65 doi 10.1016/j.it.2016.09.006. [PubMed: 27793569]
26. Barry KC, Hsu J, Broz ML, Cueto FJ, Binnewies M, Combes AJ, et al. A natural killer-dendritic cell axis defines checkpoint therapy-responsive tumor microenvironments. Nature medicine 2018;24(8):1178–91 doi 10.1038/s41591-018-0085-8.
27. Bottcher JP, Bonavita E, Chakravarty P, Blees H, Cabeza-Cabrerizo M, Sammicheli S, et al. NK Cells Stimulate Recruitment of cDC1 into the Tumor Microenvironment Promoting Cancer Immune Control. Cell 2018;172(5):1022–37 e14 doi 10.1016/j.cell.2018.01.004. [PubMed: 29429633]
28. Cheng S, Li Z, Gao R, Xing B, Gao Y, Yang Y, et al. A pan-cancer single-cell transcriptional atlas of tumor infiltrating myeloid cells. Cell 2021;184(3):792–809 e23 doi 10.1016/j.cell.2021.01.010. [PubMed: 33545035]
29. Maier B, Leader AM, Chen ST, Tung N, Chang C, LeBerichel J, et al. A conserved dendritic-cell regulatory program limits antitumour immunity. Nature 2020;580(7802):257–62 doi 10.1038/s41586-020-2134-y. [PubMed: 32269339]
30. Spranger S, Bao R, Gajewski TF. Melanoma-intrinsic beta-catenin signalling prevents anti-tumour immunity. Nature 2015;523(7559):231–5 doi 10.1038/nature14404. [PubMed: 25970248]
31. Lin JH, Huffman AP, Wattenberg MM, Walter DM, Carpenter EL, Feldser DM, et al. Type 1 conventional dendritic cells are systemically dysregulated early in pancreatic carcinogenesis. J Exp Med 2020;217(8) doi 10.1084/jem.20190673.
32. Ghislat G, Cheema AS, Baudoin E, Verthuy C, Ballester PJ, Crozat K, et al. NF-kappaB-dependent IRF1 activation programs cDC1 dendritic cells to drive antitumor immunity. Sci Immunol 2021;6(61) doi 10.1126/sciimmunol.abg3570.
33. Ouaaz F, Arron J, Zheng Y, Choi Y, Beg AA. Dendritic cell development and survival require distinct NF-kappaB subunits. Immunity 2002;16(2):257–70. [PubMed: 11869686]
34. Vonderheide RH. CD40 Agonist Antibodies in Cancer Immunotherapy. Annu Rev Med 2020;71:47–58 doi 10.1146/annurev-med-062518-045435. [PubMed: 31412220]
35. Schoenberger SP, Toes RE, van der Voort EI, Offringa R, Melief CJ. T-cell help for cytotoxic T lymphocytes is mediated by CD40-CD40L interactions. Nature 1998;393(6684):480–3. [PubMed: 9624005]
36. Diamond MS, Kinder M, Matsushita H, Mashayekhi M, Dunn GP, Archambault JM, et al. Type I interferon is selectively required by dendritic cells for immune rejection of tumors. J Exp Med 2011;208(10):1989–2003 doi 10.1084/jem.20101158. [PubMed: 21930769]
37. Blander JM. Regulation of the Cell Biology of Antigen Cross-Presentation. Annual review of immunology 2018;36:717–53 doi 10.1146/annurev-immunol-041015-055523.
38. Fuertes MB, Kacha AK, Kline J, Woo SR, Kranz DM, Murphy KM, et al. Host type I IFN signals are required for antitumor CD8+ T cell responses through CD8{alpha}+ dendritic cells. J Exp Med 2011;208(10):2005–16 doi 10.1084/jem.20101159. [PubMed: 21930765]
39. Melo-Cardenas J, Urquiza M, Kipps TJ, Castro JE. Intratumoral delivery of CD154 homolog (Ad-ISF35) induces tumor regression: analysis of vector biodistribution, persistence and gene expression. Cancer Gene Ther 2012;19(5):336–44 doi 10.1038/cgt.2012.6. [PubMed: 22402624]

40. Urquiza M, Melo-Cardenas J, Aguillon R, Kipps TJ, Castro JE. Intratumoral injection of Ad-ISF35 (Chimeric CD154) breaks tolerance and induces lymphoma tumor regression. Hum Gene Ther 2015;26(1):14–25 doi 10.1089/hum.2014.015. [PubMed: 25382101]
41. Singh M, Vianden C, Cantwell MJ, Dai Z, Xiao Z, Sharma M, et al. Intratumoral CD40 activation and checkpoint blockade induces T cell-mediated eradication of melanoma in the brain. Nat Commun 2017;8(1):1447 doi 10.1038/s41467-017-01572-7. [PubMed: 29129918]
42. Huarte E, Larrea E, Hernandez-Alcoceba R, Alfaro C, Murillo O, Arina A, et al. Recombinant adenoviral vectors turn on the type I interferon system without inhibition of transgene expression and viral replication. Molecular therapy : the journal of the American Society of Gene Therapy 2006;14(1):129–38 doi 10.1016/j.ymthe.2006.02.015. [PubMed: 16627004]
43. Larson C, Oronsky B, Scicinski J, Fanger GR, Stirn M, Oronsky A, et al. Going viral: a review of replication-selective oncolytic adenoviruses. Oncotarget 2015;6(24):19976–89 doi 10.18632/oncotarget.5116. [PubMed: 26280277]
44. Jiang H, Gomez-Manzano C, Lang FF, Alemany R, Fueyo J. Oncolytic adenovirus: preclinical and clinical studies in patients with human malignant gliomas. Curr Gene Ther 2009;9(5):422–7 doi 10.2174/156652309789753356. [PubMed: 19860656]
45. Wierda WG, Castro JE, Aguillon R, Sampath D, Jalayer A, McMannis J, et al. A phase I study of immune gene therapy for patients with CLL using a membrane-stable, humanized CD154. Leukemia 2010;24(11):1893–900 doi 10.1038/leu.2010.191. [PubMed: 20882050]
46. Wang J, Wang X, Hussain S, Zheng Y, Sanjabi S, Ouaaz F, et al. Distinct roles of different NF-kappa B subunits in regulating inflammatory and T cell stimulatory gene expression in dendritic cells. J Immunol 2007;178(11):6777–88. [PubMed: 17513725]
47. Hopewell EL, Zhao W, Fulp WJ, Bronk CC, Lopez AS, Massengill M, et al. Lung tumor NF-kappaB signaling promotes T cell-mediated immune surveillance. J Clin Invest 2013;123(6):2509–22 doi 10.1172/JCI67250. [PubMed: 23635779]
48. Stuart T, Butler A, Hoffman P, Hafemeister C, Papalexi E, Mauck WM 3rd, et al. Comprehensive Integration of Single-Cell Data. Cell 2019;177(7):1888–902.e21 doi 10.1016/j.cell.2019.05.031. [PubMed: 31178118]
49. Wolock SL, Lopez R, Klein AM. Scrublet: Computational Identification of Cell Doublets in Single-Cell Transcriptomic Data. Cell Syst 2019;8(4):281–91 e9 doi 10.1016/j.cels.2018.11.005. [PubMed: 30954476]
50. Lun AT, McCarthy DJ, Marioni JC. A step-by-step workflow for low-level analysis of single-cell RNA-seq data with Bioconductor. F1000Res 2016;5:2122 doi 10.12688/f1000research.9501.2. [PubMed: 27909575]
51. McGinnis CS, Murrow LM, Gartner ZJ. DoubletFinder: Doublet Detection in Single-Cell RNA Sequencing Data Using Artificial Nearest Neighbors. Cell Syst 2019;8(4):329–37 e4 doi 10.1016/j.cels.2019.03.003. [PubMed: 30954475]
52. Hao Y, Hao S, Andersen-Nissen E, Mauck WM 3rd, Zheng S, Butler A, et al. Integrated analysis of multimodal single-cell data. Cell 2021;184(13):3573–87 e29 doi 10.1016/j.cell.2021.04.048. [PubMed: 34062119]
53. Blondel VD, Guillaume J-L, Lambiotte R, Lefebvre E. Fast unfolding of communities in large networks. Journal of Statistical Mechanics: Theory and Experiment 2008;2008(10):P10008 doi 10.1088/1742-5468/2008/10/p10008.
54. Subramanian A, Tamayo P, Mootha VK, Mukherjee S, Ebert BL, Gillette MA, et al. Gene set enrichment analysis: a knowledge-based approach for interpreting genome-wide expression profiles. Proc Natl Acad Sci U S A 2005;102(43):15545–50 doi 10.1073/pnas.0506580102. [PubMed: 16199517]
55. Ashburner M, Ball CA, Blake JA, Botstein D, Butler H, Cherry JM, et al. Gene ontology: tool for the unification of biology. The Gene Ontology Consortium. Nat Genet 2000;25(1):25–9 doi 10.1038/75556. [PubMed: 10802651]
56. Achar SR, Bourassa FXP, Rademaker TJ, Lee A, Kondo T, Salazar-Cavazos E, et al. Universal antigen encoding of T cell activation from high-dimensional cytokine dynamics. Science 2022;376(6595):880–4 doi doi:10.1126/science.abl5311. [PubMed: 35587980]

57. Xie M, Zheng H, Madan-Lala R, Dai W, Gimbrone NT, Chen Z, et al. MEK Inhibition Modulates Cytokine Response to Mediate Therapeutic Efficacy in Lung Cancer. Cancer Res 2019;79(22):5812–25 doi 10.1158/0008-5472.CAN-19-0698. [PubMed: 31362929]
58. Senzer NN, Kaufman HL, Amatruda T, Nemunaitis M, Reid T, Daniels G, et al. Phase II clinical trial of a granulocyte-macrophage colony-stimulating factor-encoding, second-generation oncolytic herpesvirus in patients with unresectable metastatic melanoma. J Clin Oncol 2009;27(34):5763–71 doi 10.1200/JCO.2009.24.3675. [PubMed: 19884534]
59. Lauer UM, Beil J. Oncolytic viruses: challenges and considerations in an evolving clinical landscape. Future Oncol 2022 doi 10.2217/fon-2022-0440.
60. Ferrucci PF, Pala L, Conforti F, Cocorocchio E. Talimogene Laherparepvec (T-VEC): An Intralesional Cancer Immunotherapy for Advanced Melanoma. Cancers (Basel) 2021;13(6) doi 10.3390/cancers13061383.
61. Gibbons DL, Lin W, Creighton CJ, Rizvi ZH, Gregory PA, Goodall GJ, et al. Contextual extracellular cues promote tumor cell EMT and metastasis by regulating miR-200 family expression. Genes Dev 2009;23(18):2140–51 doi 10.1101/gad.1820209. [PubMed: 19759262]
62. Peng DH, Rodriguez BL, Diao L, Chen L, Wang J, Byers LA, et al. Collagen promotes anti-PD-1/PD-L1 resistance in cancer through LAIR1-dependent CD8(+) T cell exhaustion. Nat Commun 2020;11(1):4520 doi 10.1038/s41467-020-18298-8. [PubMed: 32908154]
63. Blair GE, Dixon SC, Griffiths SA, Zajdel ME. Restricted replication of human adenovirus type 5 in mouse cell lines. Virus Res 1989;14(4):339–46. [PubMed: 2560294]
64. Harari D, Abramovich R, Zozulya A, Smith P, Pouly S, Koster M, et al. Bridging the species divide: transgenic mice humanized for type-I interferon response. PloS one 2014;9(1):e84259 doi 10.1371/journal.pone.0084259. [PubMed: 24416207]
65. Miller BC, Sen DR, Al Abosy R, Bi K, Virkud YV, LaFleur MW, et al. Subsets of exhausted CD8(+) T cells differentially mediate tumor control and respond to checkpoint blockade. Nat Immunol 2019;20(3):326–36 doi 10.1038/s41590-019-0312-6. [PubMed: 30778252]
66. Connolly KA, Kuchroo M, Venkat A, Khatun A, Wang J, William I, et al. A reservoir of stem-like CD8(+) T cells in the tumor-draining lymph node preserves the ongoing antitumor immune response. Sci Immunol 2021;6(64):eabg7836 doi 10.1126/sciimmunol.abg7836. [PubMed: 34597124]
67. Jansen CS, Prokhnevska N, Master VA, Sanda MG, Carlisle JW, Bilen MA, et al. An intra-tumoral niche maintains and differentiates stem-like CD8 T cells. Nature 2019;576(7787):465–70 doi 10.1038/s41586-019-1836-5. [PubMed: 31827286]
68. Krishna S, Lowery FJ, Copeland AR, Bahadiroglu E, Mukherjee R, Jia L, et al. Stem-like CD8 T cells mediate response of adoptive cell immunotherapy against human cancer. Science 2020;370(6522):1328–34 doi 10.1126/science.abb9847. [PubMed: 33303615]
69. Siddiqui I, Schaeuble K, Chennupati V, Fuertes Marraco SA, Calderon-Copete S, Pais Ferreira D, et al. Intratumoral Tcf1(+)PD-1(+)CD8(+) T Cells with Stem-like Properties Promote Tumor Control in Response to Vaccination and Checkpoint Blockade Immunotherapy. Immunity 2019;50(1):195–211 e10 doi 10.1016/j.immuni.2018.12.021. [PubMed: 30635237]
70. Hudson WH, Gensheimer J, Hashimoto M, Wieland A, Valanparambil RM, Li P, et al. Proliferating Transitory T Cells with an Effector-like Transcriptional Signature Emerge from PD-1(+) Stem-like CD8(+) T Cells during Chronic Infection. Immunity 2019;51(6):1043–58 e4 doi 10.1016/j.immuni.2019.11.002. [PubMed: 31810882]
71. Anadon CM, Yu X, Hanggi K, Biswas S, Chaurio RA, Martin A, et al. Ovarian cancer immunogenicity is governed by a narrow subset of progenitor tissue-resident memory T cells. Cancer cell 2022;40(5):545–57 e13 doi 10.1016/j.ccell.2022.03.008. [PubMed: 35427494]
72. Schenkel JM, Herbst RH, Canner D, Li A, Hillman M, Shanahan SL, et al. Conventional type I dendritic cells maintain a reservoir of proliferative tumor-antigen specific TCF-1(+) CD8(+) T cells in tumor-draining lymph nodes. Immunity 2021;54(10):2338–53 e6 doi 10.1016/j.immuni.2021.08.026. [PubMed: 34534439]
73. Wu R, Ohara RA, Jo S, Liu TT, Ferris ST, Ou F, et al. Mechanisms of CD40-dependent cDC1 licensing beyond costimulation. Nat Immunol 2022;23(11):1536–50 doi 10.1038/s41590-022-01324-w. [PubMed: 36271147]

74. O'Hara MH, O'Reilly EM, Varadhachary G, Wolff RA, Wainberg ZA, Ko AH, et al. CD40 agonistic monoclonal antibody APX005M (sotigalimab) and chemotherapy, with or without nivolumab, for the treatment of metastatic pancreatic adenocarcinoma: an open-label, multicentre, phase 1b study. The lancet oncology 2021;22(1):118–31 doi 10.1016/S1470-2045(20)30532-5. [PubMed: 33387490]

75. Salomon R, Rotem H, Katzenelenbogen Y, Weiner A, Cohen Saban N, Feferman T, et al. Bispecific antibodies increase the therapeutic window of CD40 agonists through selective dendritic cell targeting. Nat Cancer 2022;3(3):287–302 doi 10.1038/s43018-022-00329-6. [PubMed: 35190724]

76. Ribas A, Medina T, Kirkwood JM, Zakharia Y, Gonzalez R, Davar D, et al. Overcoming PD-1 Blockade Resistance with CpG-A Toll-Like Receptor 9 Agonist Vidutolimod in Patients with Metastatic Melanoma. Cancer discovery 2021;11(12):2998–3007 doi 10.1158/2159-8290.CD-21-0425. [PubMed: 34326162]

77. Zhang J, Ji Z, Caushi JX, El Asmar M, Anagnostou V, Cottrell TR, et al. Compartmental Analysis of T-cell Clonal Dynamics as a Function of Pathologic Response to Neoadjuvant PD-1 Blockade in Resectable Non-Small Cell Lung Cancer. Clin Cancer Res 2020;26(6):1327–37 doi 10.1158/1078-0432.CCR-19-2931. [PubMed: 31754049]

78. Yost KE, Chang HY, Satpathy AT. Recruiting T cells in cancer immunotherapy. Science 2021;372(6538):130–1 doi 10.1126/science.abd1329. [PubMed: 33833111]

79. Huang AC, Orlowski RJ, Xu X, Mick R, George SM, Yan PK, et al. A single dose of neoadjuvant PD-1 blockade predicts clinical outcomes in resectable melanoma. Nature medicine 2019;25(3):454–61 doi 10.1038/s41591-019-0357-y.

80. Huang AC, Postow MA, Orlowski RJ, Mick R, Bengsch B, Manne S, et al. T-cell invigoration to tumour burden ratio associated with anti-PD-1 response. Nature 2017;545(7652):60–5 doi 10.1038/nature22079. [PubMed: 28397821]

81. Wu TD, Madireddi S, de Almeida PE, Banchereau R, Chen YJ, Chitre AS, et al. Peripheral T cell expansion predicts tumour infiltration and clinical response. Nature 2020;579(7798):274–8 doi 10.1038/s41586-020-2056-8. [PubMed: 32103181]

82. Yost KE, Satpathy AT, Wells DK, Qi Y, Wang C, Kageyama R, et al. Clonal replacement of tumor-specific T cells following PD-1 blockade. Nature medicine 2019;25(8):1251–9 doi 10.1038/s41591-019-0522-3.

83. Fairfax BP, Taylor CA, Watson RA, Nassiri I, Danielli S, Fang H, et al. Peripheral CD8(+) T cell characteristics associated with durable responses to immune checkpoint blockade in patients with metastatic melanoma. Nature medicine 2020;26(2):193–9 doi 10.1038/s41591-019-0734-6.

84. Valpione S, Galvani E, Tweedy J, Mundra PA, Banyard A, Middlehurst P, et al. Immune-awakening revealed by peripheral T cell dynamics after one cycle of immunotherapy. Nat Cancer 2020;1(2):210–21 doi 10.1038/s43018-019-0022-x. [PubMed: 32110781]

Synopsis

The authors show targeting DCs via the CD40 and type 1 IFN pathways generates systemic antitumor T-cell immunity in mouse models and NSCLC patients, highlighting a potential strategy for use alone or combined with T-cell targeting checkpoint inhibitors.

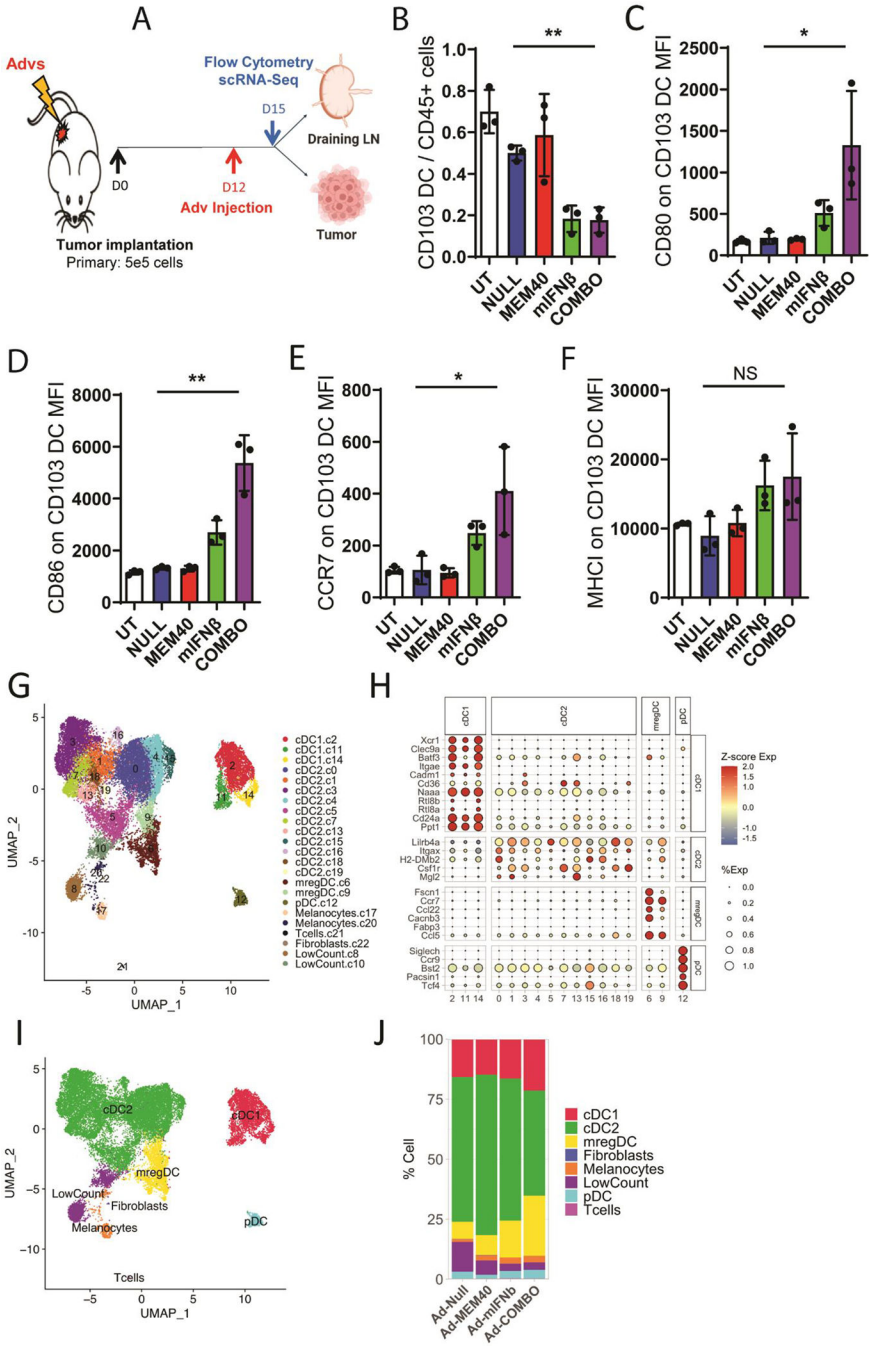

Figure 1. MEM40 and IFNβ trigger strong activation of tumor cDCs.

(A) C57BL/6 mice were inoculated s.c. with 5*e5 B16-F10 cells. On D12, mice were subjected to an intratumoral injection with $10e^9$ Ad-Null (NULL), $5\times10e^8$ Ad-Null + $5\times10e^8$ Ad-MEM40 (MEM40), $5\times10e^8$ Ad-Null + $5\times10e^8$ Ad-mIFNβ (mIFNβ) or $5\times10e^8$ Ad-MEM40 + $5\times10e^8$ Ad-mIFNβ (COMBO) (n=3 mice/treatment) 3 days after which tumors (or draining lymph nodes, Figure 2) were used for flow cytometry or scRNA-seq. (B) Proportion of $CD11c^+MHC\text{-}II^+CD103^+$ cDC1 among $CD45^+$ cells and (C-F) mean fluorescence intensity (MFI) of indicated activation markers on cDC1 in individual mice 3

days after virus injection. All results are expressed as the means ± SEM. T-test was used to determine significance of differences compared to Ad-Null treated tumors and indicated by p-values (*p<0.05, **p<0.01), NS: not significant. Ad-Null and Ad-MEM40 were not significantly different. Representative results of 1 out of 2 independent experiments are shown. (G) UMAP projections of MHC-II^{+}CD11c^{+} sorted cells showing 23 clusters colored and labeled by cell types. (H) Bubble plot of selected DC subtype markers genes in DC clusters. Color of dot represents Z-score normalized gene expression in each cluster from high (red) to low (blue). Size of dot represents the percentage of positive cells in each cluster. (I) UMAP projections of MHC-II^{+}CD11c^{+} sorted cells showing major cell types. (J) percentage composition of cell types after the indicated treatments.

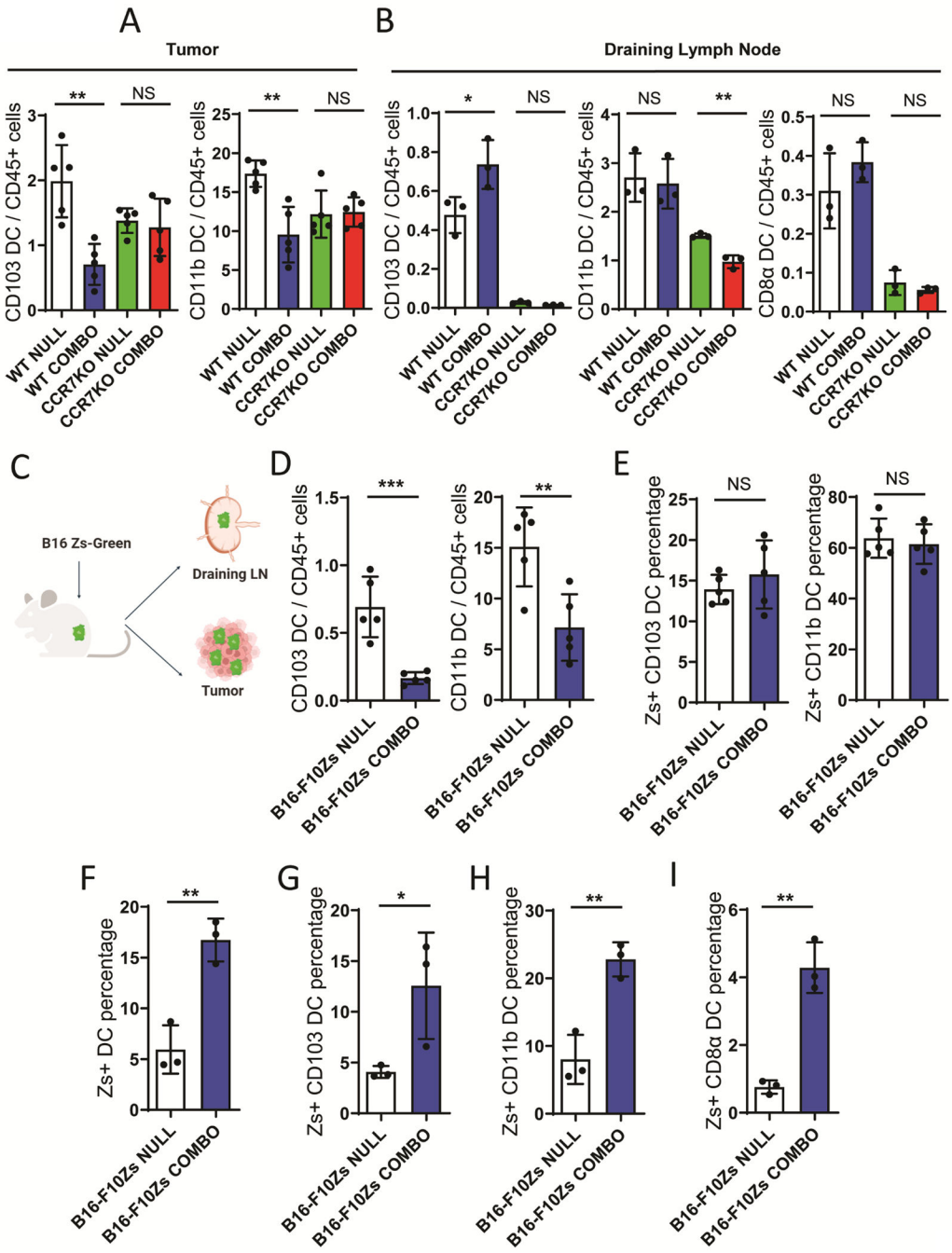

Figure 2. MEM40 + IFNβ promotes tumor DC trafficking and activation in draining lymph nodes.

(A) WT and CCR7$^{-/-}$ C57BL/6 mice were inoculated s.c. with 5*e5 B16-F10 cells. On D12, mice were subjected to an intratumoral injection with indicated viruses. Presence of CD11c^{+}MHC-II^{+}CD103^{+} cDC1 and CD11b^{+} cDC2 in tumors were determined 3 days after virus injection. (B) Pooled LNs of mice injected with indicated viruses in (A) were used to determine levels of indicated DC subsets: CD103^{+} cDC1, CD11b^{+} cDC2, and CD8α^{+} cDC1. (C) C57BL/6 mice were injected with Zs-Green expressing B16-F10 following which Zs-Green^{+} and Zs-Green^{-} tumor and LN DCs were determined. (D) Presence of CD103^{+}

cDC1 and CD11b^{+} cDC2 in tumors were determined 3 days after virus injection. (E) Percentage of Zs-Green^{+} CD103^{+} cDC1 and CD11b^{+} cDC2 in tumors were determined out of total cDC1 or cDC2. (F) Percentage of Zs-Green^{+} in total DCs, (G) CD103^{+} cDC1, (H) CD11b^{+} cDC2 and (I) CD8α^{+} cDC1 in LNs were determined. Representative results of 1 out of 2 independent experiments are shown. T-test was used to determine significance of differences and indicated by p-values *p<0.05, **p<0.01, ***p<0.001. NS: not significant.

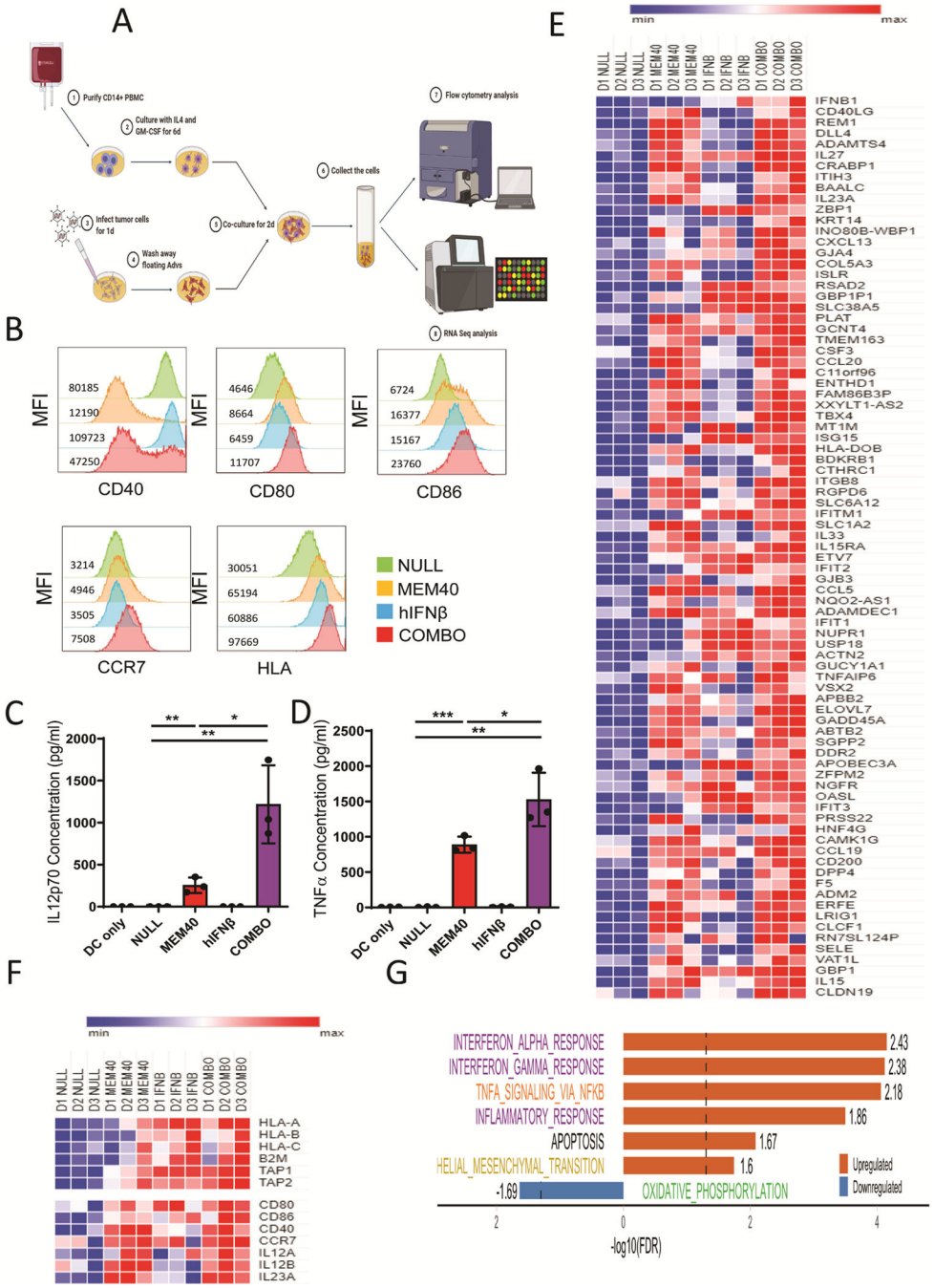

Figure 3. Distinct and synergistic impact of MEM40 and IFNβ on human DC activation markers.

(A) A549 were infected (with Ad-Null (NULL), Ad-MEM40 (MEM40), Ad-hIFNβ (hIFNβ) or Ad-MEM40 + Ad-hIFNβ (COMBO) at MOI=10 followed by cocultured with human Mo-DCs ($CD14^+$ PBMC were purified and stimulated by IL-4 and GM-CSF for 6 days). 2 days later, all cells were collected for flow cytometry analysis. (B) The expression level of DC markers on the $HLA\text{-}DR^+CD11c^+$ population are shown along with the mean florescence intensity (MFI) from a single human donor. Results are representative of findings from 2 different donors. (C-D) Secretion of IL12p70 (C) and TNFα (D)

was detected by ELISA (n=3). in the supernatant in same cells used for flow cytometry. Representative results of 1 out of 2 independent experiments are shown. All results are expressed as the means ± SEM. Statistical significance was determined by t-test and is indicated as *p<0.05, **p<0.01, ***p<0.001. NS: not significant. (E) RNA-seq was used to determine changes in gene expression after indicated treatments in HLA-DR^{+}CD11c^{+} sorted DCs derived from monocytes of 3 healthy donors. DC treatment was as in “A”. Heatmap analysis of top ~80 named genes induced in COMBO vs. Ad-Null virus treatment is shown along with individual Ad-MEM40 and Ad-IFNβ treatments. The detection of *IFNB1* and *CD40LG* is likely from contaminating A549 cells in the sorted HLA-DR^{+}CD11c^{+} population. (F) Heatmap analysis is shown of indicated DC function and activation marker genes. (G) Hallmark pathways analysis of RNA-seq showing differential pathway activation in COMBO vs. Null treatments. Normalized enrichment scores (NES) and FDR controlled p-values are indicated.

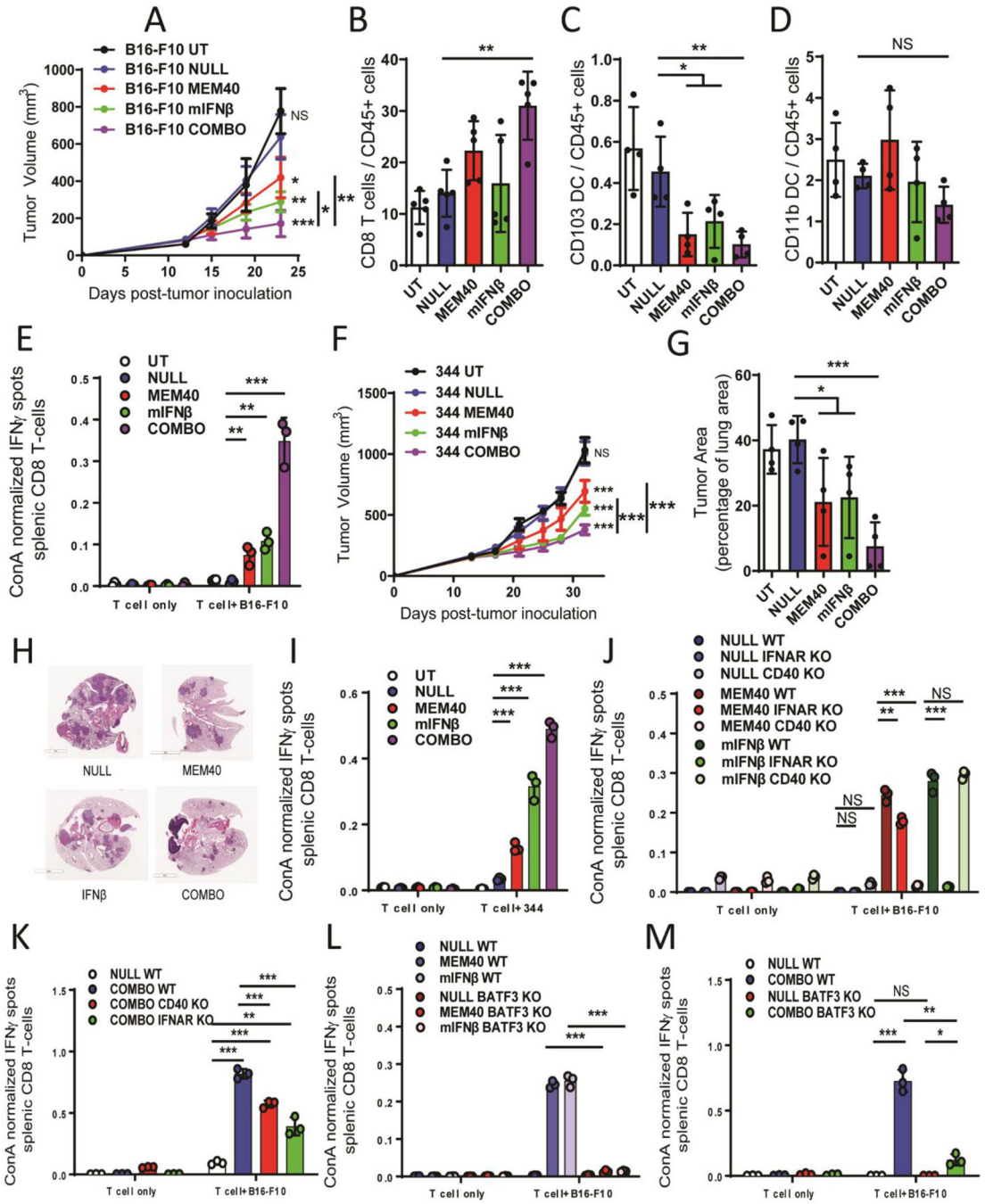

Figure 4. Combined CD40 and type 1 IFN pathway activation in the TME promotes systemic antitumor T-cell responses: impact of CD40, IFNAR1 or BATF3 deficiency.

(A) C57BL/6 mice were inoculated s.c. with 5*e5 B16-F10 cells (n=5–6 per condition). On D12 and 16, these mice were subjected to $10e^9$ Ad-Null (NULL), $5\times10e^8$ Ad-Null + $5\times10e^8$ Ad-MEM40 (MEM40), $5\times10e^8$ Ad-Null + $5\times10e^8$ Ad-mIFNβ (mIFNβ) or $5\times10e^8$ Ad-MEM40 + $5\times10e^8$ Ad-mIFNβ (COMBO). PBS injection was used in untreated (UT) group. Significance of tumor growth difference was calculated using two-way ANOVA followed by Tukey multiple comparison test. *P-value was determined in comparison with Ad-Null group. The COMBO treatment also resulted in significantly reduced tumor growth

compared to the individual MEM40 and IFNβ treatments (two-way ANOVA followed by Tukey's multiple comparisons test indicated by vertical lines). (B-D) Percentage of $CD8^+$ T cells, $CD103^+$ cDC1 and $CD11b^+$ cDC2 among live $CD45^+$ cells in the tumor are shown following flow cytometry. (E) IFNγ ELISPOT of $CD8^+$ T cells from spleens of mice (n=3) were cultured alone (T cells only) or with B16-F10. ELISPOT was performed 4 days after the second virus infection. The release of IFNγ by T cells was normalized to ConA treatment–induced release of IFNγ in the same sample T cells. Significance of difference was calculated using t-test. (F) 129 mice (n=4–6) were inoculated s.c. with 5*e5 344SQ cells (indicated as 344) and treated as mice in (A). *P-value (ANOVA) was determined in comparison with Ad-Null group. The COMBO treatment also resulted in significantly reduced tumor growth compared to the individual MEM40 and IFNβ treatments (two-way ANOVA followed by Tukey's multiple comparisons test indicated by vertical lines). (G) Quantification of tumor burden of lung metastases in mice from "F" out of total lung area. (H) Typical H&E staining of tumors in lungs metastasized from the flank tumor of the mice. (I) Quantification of IFNγ ELISPOT from spleen $CD8^+$ T cells of the 344SQ tumor–bearing mice at D22. (J) C57BL/6 background WT, $CD40^{-/-}$, and $IFNAR1^{-/-}$ mice were inoculated s.c. with B16-F10 cells. IFNγ ELISPOT of $CD8^+$ T cells from spleens of mice (n=3) were cultured alone (T cell only) or with B16-F10. ELISPOT was performed 4 days after the second virus infection. Individual virus injections were used. (K) COMBO virus was used in WT, $CD40^{-/-}$ and $IFNAR1^{-/-}$ mice. (L) Treatment with individual viruses or (M) COMBO virus in $BATF3^{-/-}$ mice. Significance of difference was calculated using t-test. Representative results of 1 out of 2 independent experiments are shown. All results are expressed as the means ± SEM. Statistical significance is indicated by p-values or as *p<0.05, **p<0.01, ***p<0.001. NS: not significant.

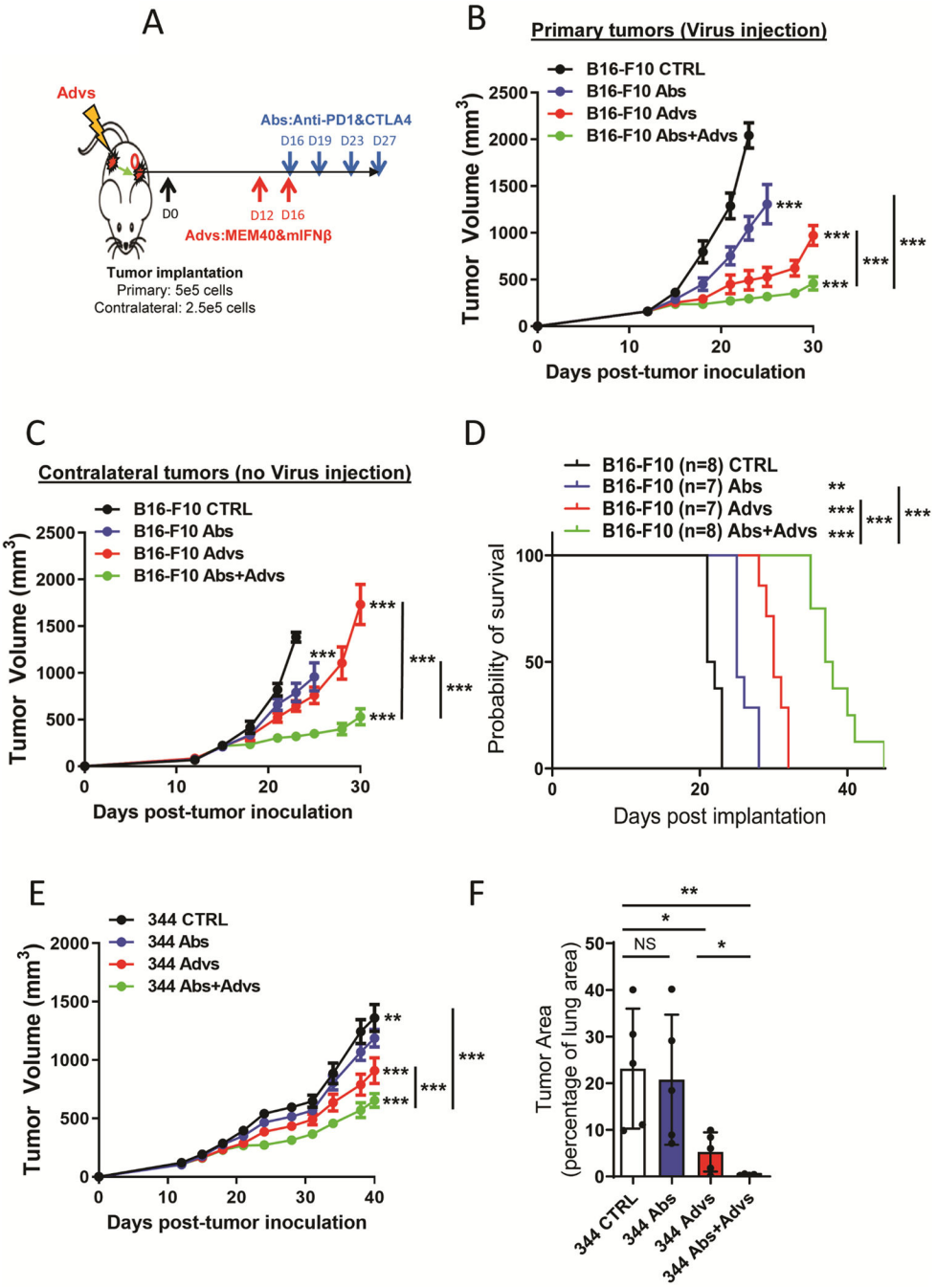

Figure 5. Combination of MEM40 + IFNβ and ICIs enhances abscopal antitumor response.

(A) Treatment regimen used in B16-F10 tumor bearing mice (n=7–8). Mice were injected with Ad-MEM40 + Ad-mIFNβ (Advs COMBO), anti-PD-1 (250 ug/mouse) and anti-CTLA-4 (100 ug/mouse) antibodies (Abs) or isotype control antibody (B16-Con) i.p. as indicated. (B-C) Tumor growth was determined on the primary site and contralateral site as indicated. Significance of tumor growth difference was calculated using two-way ANOVA followed by Tukey multiple comparison test. P-value was determined in comparison to CTRL group. Two-way ANOVA followed by Tukey's multiple comparisons test show

differences in individual treatment indicated by vertical lines. (D) Kaplan-Meier survival analysis showing overall survival of the mice in the experiment in (A). P-value was calculated by Mantel-Cox test. (E) 344SQ tumor–bearing mice were subjected to treatments as in (B) (n=4–6). (F) Quantification of tumor burden of lung metastases in mice from (E). All results are expressed as the means ± SEM. Statistical significance is indicated by p-values or as *p<0.05, **p<0.01, ***p<0.001. NS: not significant.

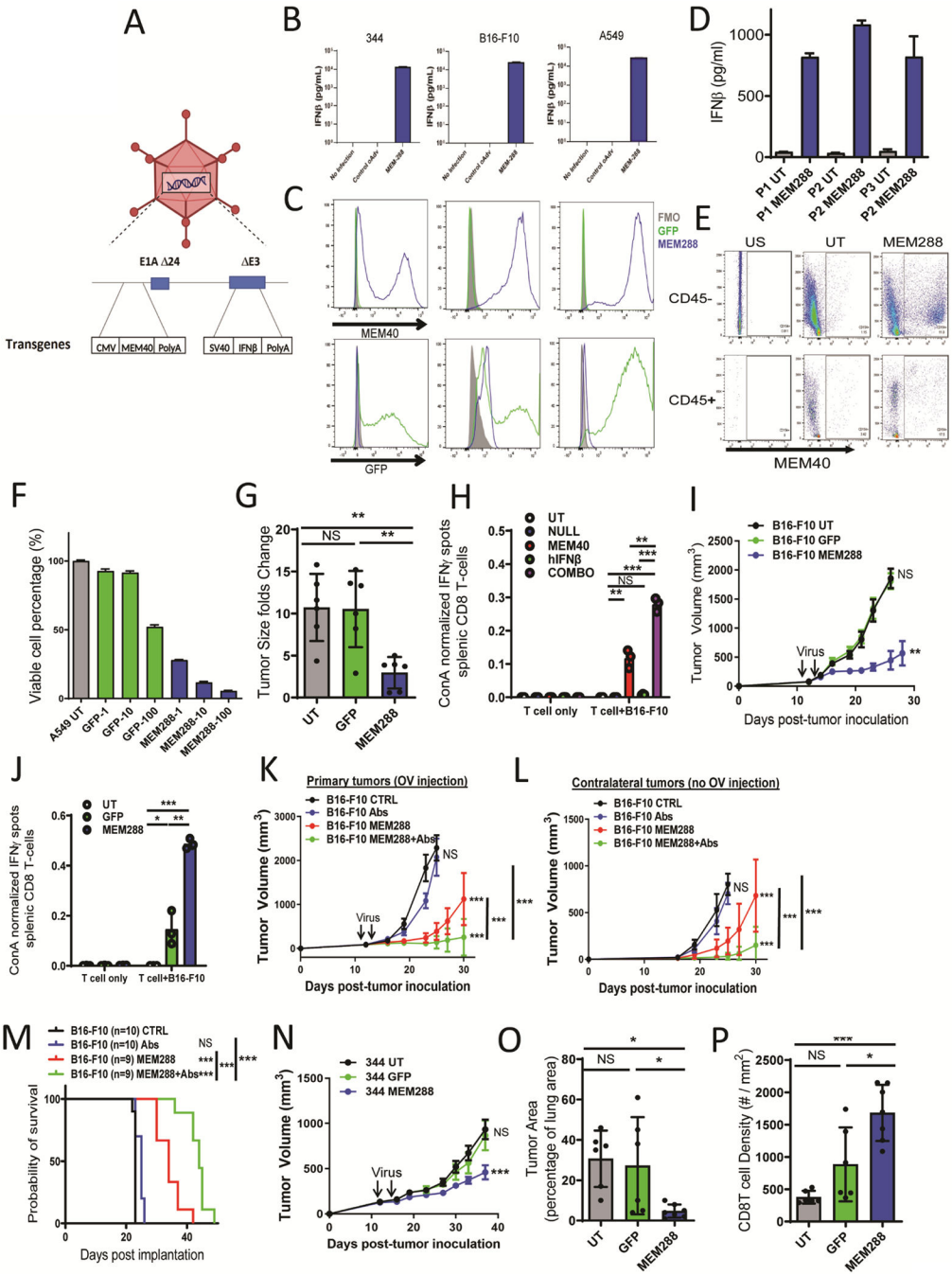

Figure 6. Generation and *in vivo* testing of MEM-288 oncolytic adenovirus.

(A) Schematic representation of MEM-288. (B-C) 344SQ, B16-F10 mouse cell lines and A549 human cell line were infected with OVs Ad-GFP (GFP) or MEM-288 (288) (MOI=10), secretion of IFNβ was detected by ELISA (B) and MEM40 and GFP was detected by flow cytometry (C). (D-E) Freshly resected human NSCLC tumors were injected with MEM-288. Secretion of IFNβ was detected by ELISA (D) and MEM40 was detected in $CD45^-$ and $CD45^+$ cells by flow cytometry (E). (F) A549 human lung cancer cells were infected with indicated OVs Ad-GFP (GFP) or MEM-288 (288) at different indicated MOIs

(1, 10, 100) for 2 days. Cell viability was determined by trypan blue staining assay. (G) A549-luciferase expressing tumors in SCID mice were injected with 2 injections of 10e9 of Ad-GFP or MEM-288 (one week apart) and bioluminescence imaging (BLI) was used to detect tumor growth over 3 weeks. Quantification of the change in BLI signal from before virus injection is shown. (H) IFNγ ELISPOT was performed using spleen $CD8^+$ T cells after injection of B16-F10 tumors with replication-deficient Ad-(human) hIFNβ, Ad-MEM40 and the combination. (I) B16-F10 tumors were injected with oncolytic Ad-GFP or MEM-288 at 10e9 IU on D12 and 16 into the tumors (n=9). Significance of tumor growth difference was calculated using two-way ANOVA. (J) Quantification of IFNγ ELISPOT using spleen $CD8^+$ T cells 4 days after the second virus infection. (K-L) Treatment regimen was as in Fig. 5A (n=9–10 per group). Mice were injected with MEM-288 at 10e9 IU on D12 and 16 into primary tumors and with anti-PD-1 and anti-CTLA-4 i.p. on D16, D19, D23 and 27. Two-way ANOVA followed by Tukey's multiple comparisons test show differences in individual treatment indicated by vertical lines. (M) Kaplan-Meier survival nalysis showing overall survival of the mice. P-value was calculated by Mantel-Cox test. (N) 129 mice were inoculated s.c. with 5*e5 344 cells on the flank and subjected to oncolytic Ad-GFP, or MEM-288 at 10e9 IU on D12 and 16 into the tumors (n=6–7 per group). Tumor growth was determined on the primary site as indicated. (O) Quantification of tumor burden of lung metastases out of total lung area. (P) Quantification of $CD8^+$ T-cell density in tumor indicated out of mm^2 of tumor area. All results are expressed as the means ± SEM. Statistical significance was determined by t-test and is indicated by p-values or as *p<0.05, **p<0.01, ***p<0.001. NS: not significant.

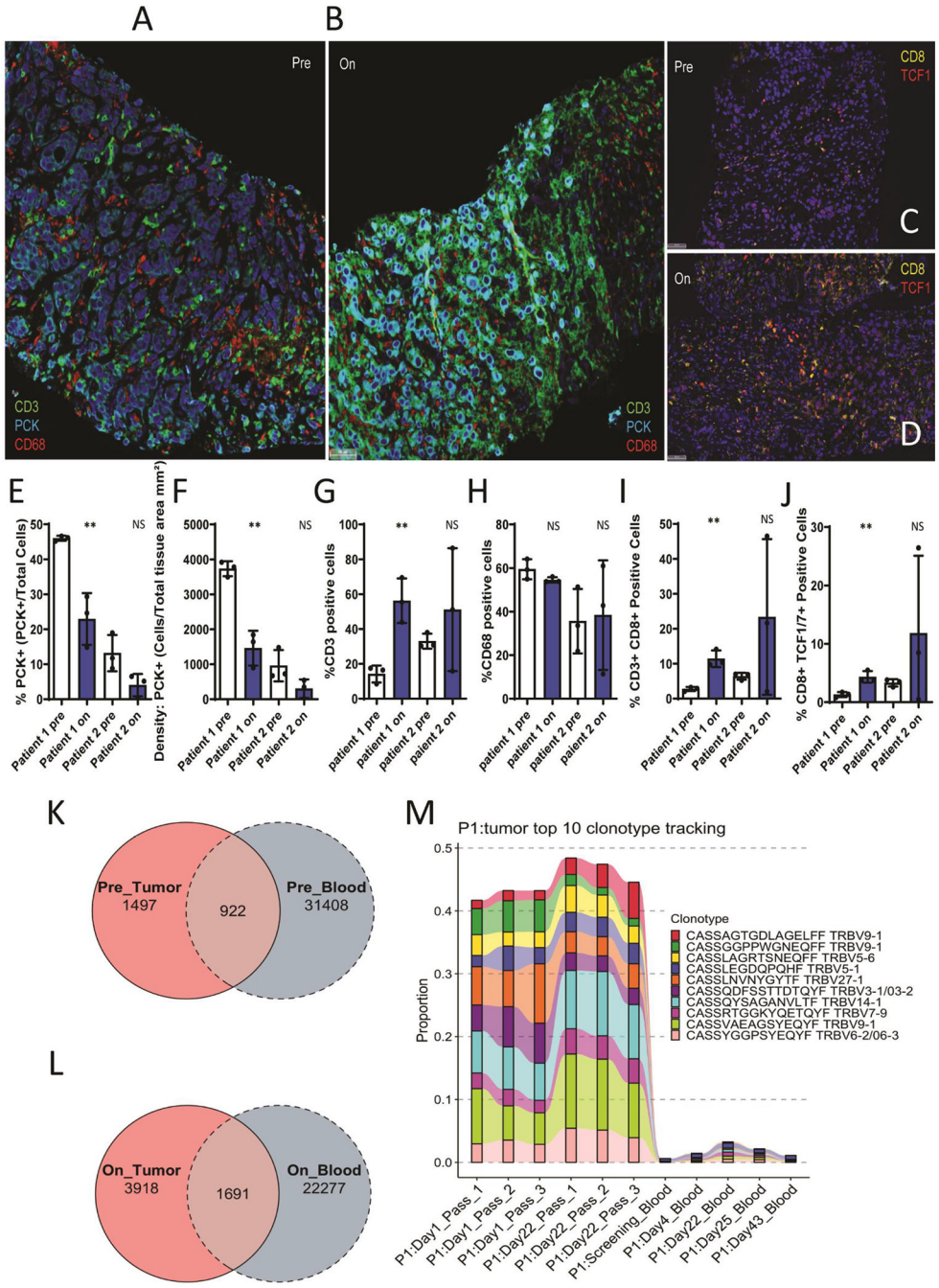

Figure 7. MEM-288 modulation of the TME and systemic T-cell immunity in NSCLC.

(A-D) mIF was performed using pre- and on-treatment biopsies with indicated markers and DAPI on 2 patients. (E-J) Changes in PCK^+ cell percentage and density, and percentage of indicated cell types out of total $DAPI^+$ cells in pre- and on-treatment tumors. All results (n=3) are expressed as the means ± SEM. Statistical significance was determined by t-test and is indicated by p-values or as *p<0.05, **p<0.01, ***p<0.001. NS: not significant. (K-L) Shared clonotypes between tumors (all 3 passes), tumor and blood, and total blood clonotypes pre-treatment and on-treatment. (M) Top-10 tumor clonotypes in

pre-treatment and on-treatment biopsies of 1 patient were tracked in peripheral blood at indicated timepoints.